A Semi-Automated, High Throughput Method for Genetically Engineering and Phenotyping Yeast Extracellular Vesicles

Kathleen Hon

A Thesis in The Department of Biology

Presented in Partial Fulfillment of the Requirements
for the Degree of Master of Science (Biology)

at Concordia University
Montréal, Québec, Canada

August 2025

CONCORDIA UNIVERSITY
School of Graduate Studies

This is to certify that the thesis prepared

By: Kathleen Hon

Entitled: A Semi-Automated, High Throughput Method for Genetically Engineering and Phenotyping Yeast Extracellular Vesicles

and submitted in partial fulfillment of the requirements for the degree of

Master of Science (Biology)

complies with the regulations of the University and meets the accepted standards with respect to originality and quality.

Signed by the final examining committee:

_____ Chair
Dr. William Zerges

_____ Examiner
Dr. Vincent Martin

_____ Examiner
Dr. Alisa Piekny

_____ Examiner
Dr William Zerges

_____ Thesis Supervisor
Dr. Christopher Brett

Approved by _____
Dr. Robert Weladji, Graduate Program Director

Date: August 29, 2025 _____
Dr. Pascale Sicotte, Dean of Faculty of Arts and Science

Abstract

A Semi-Automated, High Throughput Method for Genetically Engineering and Phenotyping Yeast Extracellular Vesicles

Kathleen Hon

Extracellular vesicles (EVs) represent a promising new modality for drug delivery. We use *Saccharomyces cerevisiae* (baker's yeast) – an organism used for drug biomanufacturing – as a platform to design, build, and test engineered EVs for therapeutic applications. This involves modifying their contents and surfaces by adding human or yeast proteins with diverse functionalities requiring testing of thousands of modifications (individually or in combination) to optimize EV cargo loading, cell targeting, and content delivery, tailoring to specific outcomes in patients. To support our studies, I sought to establish high-throughput cloning and phenotyping protocols to generate libraries of genetically modified *S. cerevisiae* strains. I employed Golden Gate and Gateway cloning strategies based on the modular Yeast Toolkit, enabling use of new constructs by the synthetic biology community. Candidate genes were introduced into donor plasmids and then integrated into expression vectors containing a strong promoter (TDH3) and the Nanoluciferase (NLuc) gene. PCR, genetic assemblies, bacterial transformations and colony selection were conducted in 96-well plate format by robotic equipment housed in Concordia University's Genome Foundry. After assembled vectors were validated by pooled nanopore sequencing, robots were used to transform them into *S. cerevisiae* (e.g. wild type BY4741), to select clonal transformants, and to prepare furizamine-based assays for detection of candidate proteins tagged with the luminescent biomarker nanoluciferase (NLuc) within whole cell lysates or EV-containing samples, measured using a plate-reading luminometer. As proof-of-concept, I implemented an automated procedure to generate an initial set of 96 yeast strains each expressing

a candidate protein fused to (NLuc). Despite using a single promoter, I observed variable expression levels of human and yeast candidate proteins within *S. cerevisiae* cells. Initial phenotyping of extracellular media containing EVs revealed the presence of some protein candidates, later confirmed by assessing EVs purified by ultrafiltration and size exclusion chromatography. These included human proteins (e.g. CD81), suggesting that the mechanism(s) underlying EV protein loading are conserved. In all, I developed an automated yeast genetic engineering and phenotyping research pipeline for high-throughput screening of strategies to improve EV functionalities required for use as next-gen drug delivery vehicles.

Acknowledgements

I would like to thank Dr. Brett for the opportunity to pursue research in his lab. He has been an exceptional supervisor, mentor, and I am deeply grateful for his guidance, patience, and unwavering support throughout my project. He's inspired me to be a better scientific communicator and has provided me with so many amazing experiences in my Master's that I will cherish.

I'd like to thank Dr. Jeff Bouffard for his patience in teaching me the fundamentals of cloning and for equipping me with the proper tools to do science with both precision and care. I will never forget my first few months, spending hours back and forth on Geneious, figuring out how to mutate-out internal cut sites, how to hold a pipette correctly and even opening tubes with one hand. I'd like to thank all the other members of my lab for lending a helping hand whenever I needed: Curt Logan, for helping me with EV isolations and NTA data, Devina Singh for helping me troubleshoot in my early days of cloning, Joseph Trani for showing me useful databases, and Derin Gokbayrak for always lending me reagents when I've run low.

A heartfelt thank you goes to the members of the Concordia Genome Foundry. I especially want to thank Nicholas Gold for his generosity with his time and for helping me draft the initial blueprint of the project. As well as James Bagley, who played a key role in the early stages of my project and took the time to train me on all the equipment at the Foundry. Angela Quach, whose responsiveness and support were invaluable after James's departure, and to Jing Cheng for sharing her extensive cloning knowledge and efficient plasmid validation strategy, which saved me a great deal of time. My project could not have happened without you all.

I want to thank my lab bestie, Julia De Le Garza, for being my constant through every experiment, deadline, and existential crisis I've gone through during my time here. From troubleshooting protocols to celebrating the smallest wins (and occasionally spiralling together over failed transformations), your support, humour, and unshakable optimism made every long day in the lab not only bearable but fun. I'd also like to thank all the amazing women in the other labs of the GE building who've worked alongside me every day, who've kept me inspired to stay curious and pursue scientific research.

Last but not least, I want to thank my parents for their unwavering support throughout my Master's journey and especially for Mom providing the stability and generous support I needed in my personal life which has granted my focus into this project and my graduate studies. To my sister Casey for her words of encouragement and occasional trips when I felt homesick and my wonderful dog Cooper whose face never fails to brighten my day.

Table of Contents

List of Figures

List of Tables

List of Abbreviations

BBB – Blood-Brain Barrier
CARB – carbenicillin
CDS – coding sequence
extracellular media – extracellular media
EGFR – epidermal growth factor receptor
ESCRT – endosomal sorting complex required for transport
EV – extracellular vesicle
GPI – Glycosyl phosphatidyl inositol
GRAS – generally recognized as safe
HSP – heat shock protein
ILV – intralumenal vesicle
KAN - kanamycin
LiOAc – lithium acetate
MMP1 – matrix metalloprotease 1
µl – microliters
µm – micrometers/microns
MoClo – modular cloning
MoClo-YTK – modular cloning yeast toolkit
MVB – multivesicular body
NLuc – nanoluciferase
nm – nanometers
NTA – nanoparticle tracking analysis
O/N – overnight
OD600 – optical density at 600nm
OD – optical density
PBS – phosphate buffer saline
PEG – polyethylene glycol
PM – plasma membrane
Rapa – rapamycin
SC – synthetic complete
SD – standard deviation
SD-URA – synthetic defined (media) without uracil
SEC – size exclusion chromatography
S.E.M – standard error of means
SPEC – spectinomycin
Tluc – ThermoLuciferase
YPD – yeast peptone dextros

Introduction

1.1 What are Extracellular Vesicles?

Extracellular vesicles (EVs) are membrane-bound nanoparticles naturally released by cells across species across all domains of life. EVs carry bioactive molecules that facilitate intercellular communication and play key roles in both physiological and pathological processes (Sanghvi et al., 2025). In animals, EVs travel systemically for targeted intercellular signalling and have been shown to mediate interspecies communication (Luo et al., 2020, Chen et al., 2024). In human cells, EVs have been shown to maintain homeostatic processes (e.g stress responses) as well as regulate blood pressure, learning and memory, immune responses, tissue regeneration, and bone remodelling (Lachenal et al., 2011, Kang et al., 2020, Shi et al., 2021). Briefly, an EV's journey begins with biogenesis within a donor cell, followed by triggered release into the extracellular milieu, where it may travel long distances before uptake by a target cell primarily via endocytosis. Upon delivery, EV cargo – proteins, lipids, nucleic acids – trigger profound cellular responses underlying related physiology.

EVs can be broadly categorized into ectosomes, which bud directly from the plasma membrane, and exosomes, which originate within multivesicular bodies (MVBs). Exosomes are formed when the membrane of an endosome buds inward to form intraluminal vesicles. As intralumenal vesicles accumulate, the endosome matures into an MVB. Intralumenal vesicles are then secreted as exosomes when the MVB fuses with the plasma membrane (Lasser et al., 2012). Through the exosomal biosynthetic pathway, cargoes in the form of proteins, lipids, and nucleic acids are sorted into EVs in a regulated and context-specific manner (Lasser et al., 2012). One of the ways that exosomes package their cargoes is through the use of the Endosomal Sorting Complex

Required for Transport (ESCRT) machinery (Debbi et al., 2022). This machinery includes four protein complexes, ESCRT-0, ESCRT-I, ESCRT-II, and ESCRT-III, that function in sequential order to initiate and execute the biogenesis of exosomes (Hurley J & Hanson.P., 2010). ESCRT-derived exosomes typically range from 30 to 150 nm in diameter (Lasser et al., 2012). This highly controlled pathway is responsible for packaging bioactive molecules in a context-specific manner, which allows for cells to communicate with each other and function in harmony.

However, just as they help mediate physiology, EVs can equally contribute to the pathogenic processes and are implicated in cancer, neurodegenerative disorders, and cardiovascular diseases (Al-Nedawi et al., 2008, Bobdryshev et al., 2008, Pacheco-Quinto et al., 2019). For instance, tumour-derived EVs can remodel the tumour microenvironment, promote angiogenesis, suppress immune responses, and facilitate metastasis (Al-Nedawi et al., 2008). In neurodegenerative disorders, EVs are implicated in the spread of misfolded or aggregated proteins, such as amyloid-β or α-synuclein, accelerating disease progression across neuronal networks (Pacheco-Quinto et al., 2019). Endothelial- and platelet-derived vesicles can induce vascular inflammation, thrombosis, and atherosclerotic plaque formation (Bobryshev et al., 2008). Collectively, these findings reveal that EVs are dual-natured communicators: they can sustain physiological balance or act as vectors for pathological signalling.

1.2 Therapeutic and Diagnostic Potential of EVs

Over the past decade, exosomes derived from specific cell types, such as mesenchymal stem cells (MSCs), have emerged as a promising new modality for drug delivery for diverse

therapeutic strategies, with engineered variants showing enhanced ability to target diseased tissues (Ghodasara et al., 2023). This targeting is thought to be mediated by specific surface molecules on exosomes that guide them to target cells, making them very attractive candidates for drug delivery (Thery et al., 1999, Lasser et al., 2012). In 2022, Yan Lin et al. demonstrated that human umbilical cord mesenchymal stem cell (Huc-MSC)–derived exosomes engineered to display the targeting peptide HSTP1 can specifically target activated hepatic stellate cells (HSCs) (Lin et al., 2022). In vitro, these exosomes reverted activated HSCs toward an inactive phenotype, and in vivo, they selectively localized to fibrotic liver tissue and significantly reduced fibrosis. Other approaches include naturally enriching lipid raft–associated lipids and proteins, including glycosyl phosphatidyl inositol (GPI), on EV membrane,s which has been shown to improve delivery of nanobodies targeting oncogene epidermal growth factor receptor (EGFR) on the surface of various tumour cell lines (Kooijmans et al., 2016).

Given the issues in cell-specific delivery of therapeutic compounds in the pharmaceutical industry, EVs are a hopeful solution. Indeed, many of their features qualify them as a strategic avenue for delivery of therapeutics, including their abilities to use the cell machinery to load specific cargoes, to selectively target cells and tissues, to cross the blood-brain barrier, and to evade immunogenicity (Smyth et al., 2015, Banks et al., 2020). Their capacity to carry therapeutics is particularly appealing for protein, RNA and DNA–based drugs, which are especially sensitive to fluctuations in temperature, solvents, pH, extracellular degradation by enzymes, and unable to cross the plasma membrane (Fast et al., 2024). Alvarez-Erviti et al. (2011) were the first to demonstrate that exosomes administered in mice can cross the BBB and deliver siRNA to neurons, microglia, and oligodendrocytes in the brain for gene knockdown

(Alvarez-Erviti et al., 2011). Since then, EVs have been used to successfully deliver various therapeutic molecules. For example, EVs were used to deliver doxorubicin – a chemotherapeutic agent – in tumour-bearing mice to promote drug accumulation at tumour sites, reducing systemic toxicity compared to free drug administration (Tang et al., 2022). EVs loaded with rapamycin (Rapa) – an mTOR pathway inhibitor – were administered to glioblastoma multiforme mouse models to improve blood-brain barrier penetration and prolong therapeutic retention in brain tumour tissue (Song et al., 2025). These preclinical studies highlight the unique ability of EVs to function as biocompatible drug carriers capable of overcoming pharmacokinetic and biodistribution limitations of conventional therapies.

In a clinical context, EV-based therapeutics are beginning to make their way from bench to bedside. Johnson et al., (2023) were the first to test the clinical safety and efficacy of a single injection of EVs in skin lesions using clinical-grade platelet-derived EVs and proved EV injections are safe to healthy individuals in the context of wound healing (Johnson et al., 2023). More recently, a Phase I trial using MSC-derived exosomes loaded with KRAS^G12D siRNA for the treatment of pancreatic cancer demonstrated good tolerability among patients (Lebleu et al., 2025). These trials not only provide proof-of-concept evidence for EVs as a viable therapeutic platform but also set the stage for future therapeutic applications involving targeted RNA delivery, combination therapies, and personalized EV-based interventions.

1.3 Challenges with Clinical Translation of EVs

EV research has been primarily focused on human-derived EVs, especially from mesenchymal stem cell (MSC) sources, because they've been shown to carry intrinsic anti-inflammatory cargoes (Yang et al., 2015, Wu et al., 2019, Nguyen et al., 2024). However, there are caveats in advancing MSC-derived EVs for therapeutic potential, as there are challenges in the isolation process and engineering them to load specific cargoes (He et al., 2024). EVs can be loaded exogenously by electroporation or by endogenous approaches like genetic engineering (Obuchi et al., 2025, Elashiry et al., 2020). Both exogenous and endogenous methods have proven effective at loading RNAs, proteins, and lipids; however, exogenous methods face issues of compromising EV membrane integrity (Chen et al., 2024, Rankin-Turner et al., 2021). Endogenous loading mechanisms require fusing the protein of interest to a scaffold protein that can shuttle or anchor the cargo of interest to the EV during biogenesis at the MVB. Common scaffold proteins used for cargo loading include those involved in the ESCRT pathway, e.g. ALIX, or resident EV membrane proteins such as CD9, CD81, and CD63 (Lavello et al., 2016, Heath et al., 2019, Obuchi et al., 2025).

A review by Herrmann et al. (2021) highlights that although developing new EV-based therapies up to the preclinical stage is highly feasible, large-scale EV purification and large batch drug loading required for clinical applications are limiting (Herrmann et al., 2021). Specifically, to bring EV-based therapies to the clinic, they must be derived from a standardized cell line, which typically means establishing an immortalized mammalian cell line, to limit batch-to-batch variability and help ensure biocompatibility. Indeed, many reviews on potential clinical use of exosomes have raised parallel concerns about the translation of MSC-derived exosome therapies, and bring up other issues such as the inability to scale up exosome production, difficulties with

clinical-grade purification to homogeneity, and storage (Mendt et al., 2019). In addition, current methods for bioproduction of MSC-derived EVs are incredibly costly (Claridge et al., 2021). This highlights the need for research in these areas to eventually realize clinical use of EVs.

1.4 Yeast EVs as a Therapeutic Platform

Despite extensive research on MSC-derived EVs, their clinical translation is constrained by many barriers, demonstrating the need for alternative platforms to biomanufacture EV-based therapeutics that offer greater standardization and engineering control (Ma et al., 2024). To address this, our team has developed *Saccharomyces cerevisiae*, baker's yeast, as a platform for designing, engineering, testing and bioproducing customized EVs for therapeutic applications. *S. cerevisiae* offers several advantages: it releases high amounts of EVs and possesses orthologs of the biogenesis machinery, i.e. ESCRTs, it produces EVs with reduced ectosomal heterogeneity, and it is highly amenable to genetic manipulation (Zhao K., et al., 2019). Previous work from our lab showed that heat stress triggers EV production and release from *S. cerevisiae*, like human cells (Bewicke-Copley et al., 2017), and their EVs confer thermotolerance to neighbouring cells, enhancing survival under otherwise lethal conditions (Logan et al., 2022). In addition, Jeon et al., (2025) demonstrated that yeast-derived EVs are readily endocytosed by human fibroblasts, where they enhance expression of type I collagen and matrix metalloprotease 1 (MMP1) in these cells (Jeon et al., 2025).

While further research is needed to establish the clinical feasibility and functionality of yeast-derived EVs, their potential competitive advantage stems from their well-established role in industrial biomanufacturing. Notably, *S. cerevisiae* is a robust, cost-effective, genetically

tractable organism, widely used for heterologous protein expression. For decades, *S. cerevisiae* has been used to produce therapeutic natural products and biopharmaceuticals such as cytokines, blood products, vaccines, hormones, and enzymes (Duport et al., 1998, Trantas et al., 2009, Martinez et al., 2012). *S. cerevisiae* is generally recognized as safe (GRAS), further supporting suitability for clinical applications (Roohvand et al., 2017, Kulagina et al., 2021). Taken together, realization of EV-based therapies could rely on a scalable yeast bioproduction system, avoiding limitations associated with mammalian-derived sources (Kulagina et al., 2021).

1.5 EV Scaffold Proteins Matter for Therapeutic Engineering

To leverage yeast EVs for therapeutic or biotechnological applications, it is essential to identify a reliable yeast-specific EV scaffold protein. Although numerous scaffold proteins have been characterized in mammalian systems, their functionality is often highly context-dependent, and many lack orthologs in yeast (e.g. CD63). This raises a key question: how can we systematically screen for yeast-specific EV scaffold proteins in a high-throughput manner?

In a prior study, Zheng et al. (2023) screened 244 candidate scaffold proteins for EV incorporation by tagging a bioluminescent reporter to the C-terminus of each protein and expressing them across five mammalian cell types (Zheng et al., 2023). This enabled high-throughput detection of these candidate scaffolds in extracellular medium containing EVs prior to their isolation. Despite identifying 24 scaffolds, the candidates were largely restricted to tetraspanin family members, limiting the diversity of scaffold types. Building off this strategy, I sought to develop a similar high-throughput screening approach tailored to *S. cerevisiae*. I

employed NanoLuciferase (NLuc), a small (~500 bp, ~19 kDa), bright, and highly sensitive bioluminescent reporter, to help us identify EV scaffold proteins by genetically tagging 63 *S. cerevisiae* proteins and 25 human proteins and fusing them at the C-terminus to NLuc. These NLuc-tagged proteins were expressed in *S. cerevisiae,* and I evaluated their ability to sort into extracellular vesicles (Figure 1). The size of NLuc and inclusion of a small linker peptide minimizes the risk of steric hindrance or disruption of normal protein trafficking, which is particularly important when considering the relatively small volume of the vesicular lumen. Additionally, NLuc produces exceptionally bright and stable luminescence with low background, allowing sensitive detection of even a few proteins within each EV. Unlike fluorescent proteins, which require excitation and are prone to photobleaching, NLuc generates its signal enzymatically, which can be amplified, and this can be quantified directly in both cell lysates and extracellular media. Most importantly, NLuc has been validated previously as an effective EV reporter both in vitro and in vivo mammalian systems (Gupta et al., 2020) which will accommodate EV tracking in future experiments. I hypothesize that at least a subset of these candidate proteins will be effective scaffolds that we may use for therapeutic cargo loading in engineered yeast EVs for a multitude of applications.

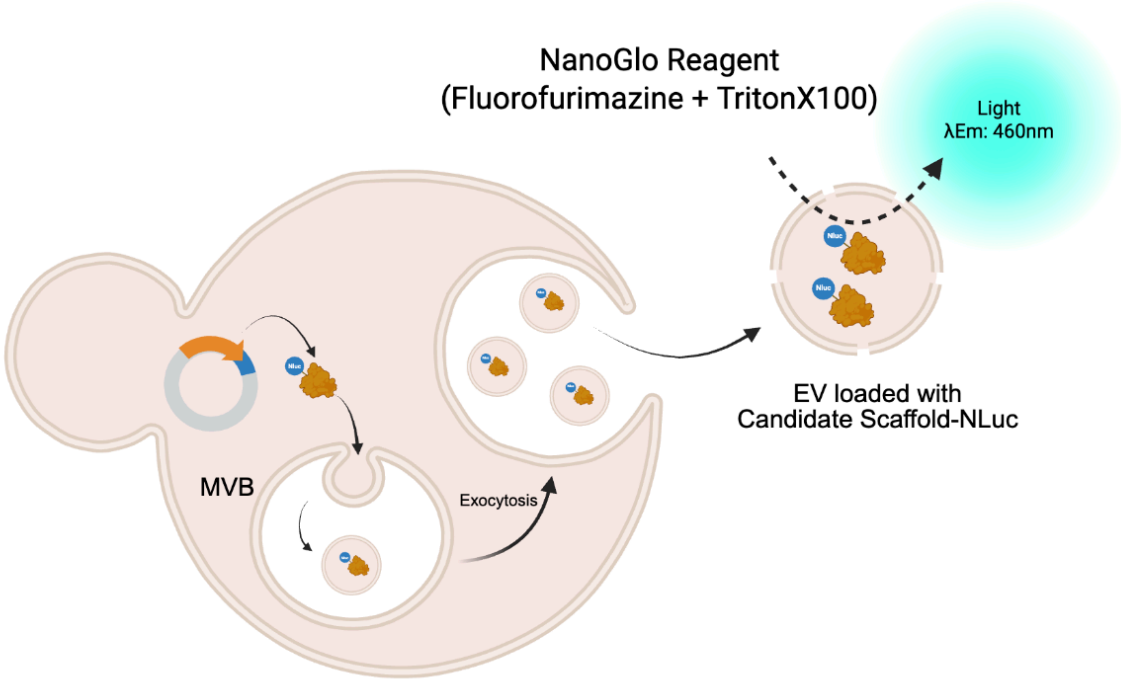
NanoGlo Reagent
(Fluorofurimazine + TritonX100)
Light
λEm: 460nm
EV loaded with
Candidate Scaffold-NLuc
MVB
Exocytosis

Figure 1. Schematic of plasmid-based expression of a candidate EV scaffold protein for engineered EVs. Candidate scaffold proteins fused to NLuc should be sorted into newly forming EV at multivesicular bodies (MVB) and then be eventually secreted into the extracellular medium through exocytosis.

1.6 Thesis Summary

This thesis describes the development of a high-throughput cloning method to engineer and phenotype protein cargoes loaded into yeast EVs, enabling rapid screening and identification of EVs with novel functionalities for therapeutic applications. My objectives are to develop a streamlined semi-automated workflow to perform these high-throughput studies and to identify an array of bona fide scaffold proteins for efficient EV cargo protein loading. For proof-of-principle, I generated a library of 88 NLuc-tagged candidate scaffold proteins from both yeast and human using a modular Golden Gate/Gateway cloning pipeline and successfully expressed 50 constructs in yeast. Screening for EV incorporation showed that intravesicular NanoLuc activity did not correlate with overall cellular expression or secretion, highlighting the need for assess purified EV samples to properly identify valid EV scaffold proteins. Purified EVs exhibited a narrow size distribution with ~120 nm median diameter, and fractionation of filtered extracellular medium by size exclusion chromatography demonstrated that human CD9-NLuc was highly enriched in the EV membranes. Together, these findings validate the use of NLuc-based phenotyping for rapid EV cargo detection and screening, and provide foundational tools for engineering yeast EVs for future therapeutic and diagnostic applications.

Materials & Methods

2.1 Yeast Strains

I used the model yeast strain BY4741 *(MATa his3-Δ1 leu2-Δ0 met15- Δ0 ura3-Δ0 Huh et al., 2003)* for all plasmid transformations. The culture media used for yeast maintenance were yeast extract, peptone, dextrose (YPD) and Synthetic Complete (SC). The transformed yeast strains were maintained on auxotrophic selection of uracil on synthetic defined (SD-URA) (Table 1).

Table 1. Yeast strains created in this study

Strain	Genotype	Source
BY4741	*MATa his3Δ1 leu2Δ0 met15Δ0 ura3Δ0*	*Huh et al. 2003*
FCER1G-NLuc	*MATa his3Δ1 leu2Δ0 met15Δ0 ura3Δ0 + [pTDH3-FCER1G-NLUC-tADH1 URA3]*	This study
SSA1-NLuc	*MATa his3Δ1 leu2Δ0 met15Δ0 ura3Δ0 + [pTDH3-SSA1-NLUC-tADH1 URA3]*	This study
PIN3-NLuc	*MATa his3Δ1 leu2Δ0 met15Δ0 ura3Δ0 + [pTDH3-PIN3-NLUC-tADH1 URA3]*	This study
YDL124W-NLuc	*MATa his3Δ1 leu2Δ0 met15Δ0 ura3Δ0 + [pTDH3-YDL124W-NLUC-tADH1 URA3]*	This study
SGT2-NLuc	*MATa his3Δ1 leu2Δ0 met15Δ0 ura3Δ0 + [pTDH3-SGT2-NLUC-tADH1 URA3]*	This study
HSPAA1-NLuc	*MATa his3Δ1 leu2Δ0 met15Δ0 ura3Δ0 + [pTDH3-HSPAA1-NLUC-tADH1 URA3]*	This study
CD81-NLuc	*MATa his3Δ1 leu2Δ0 met15Δ0 ura3Δ0 + [pTDH3-CD81-NLUC-tADH1 URA3]*	This study
ARRDC1-NLuc	*MATa his3Δ1 leu2Δ0 met15Δ0 ura3Δ0 + [pTDH3-ARRDC1-NLUC-tADH1 URA3]*	This study
TPM3-NLuc	*MATa his3Δ1 leu2Δ0 met15Δ0 ura3Δ0 + [pTDH3-TPM3-NLUC-tADH1 URA3]*	This study

Strain	Genotype	Source
GPI-NLuc	*MATa his3Δ1 leu2Δ0 met15Δ0 ura3Δ0 + [pTDH3-GPI-NLUC-tADH1 URA3]*	This study
HSP90-NLuc	*MATa his3Δ1 leu2Δ0 met15Δ0 ura3Δ0 + [pTDH3-HSP90-NLUC-tADH1 URA3]*	This study
ENO2-NLuc	*MATa his3Δ1 leu2Δ0 met15Δ0 ura3Δ0 + [pTDH3-ENO2-NLUC-tADH1 URA3]*	This study
PGK1-NLuc	*MATa his3Δ1 leu2Δ0 met15Δ0 ura3Δ0 + [pTDH3-PGK1-NLUC-tADH1 URA3]*	This study
VDBP-NLuc	*MATa his3Δ1 leu2Δ0 met15Δ0 ura3Δ0 + [pTDH3-VDBP-NLUC-tADH1 URA3]*	This study
FLOT1-NLuc	*MATa his3Δ1 leu2Δ0 met15Δ0 ura3Δ0 + [pTDH3-FLOT1-NLUC-tADH1 URA3]*	This study
DJ-1-NLuc	*MATa his3Δ1 leu2Δ0 met15Δ0 ura3Δ0 + [pTDH3-DJ1-NLUC-tADH1 URA3]*	This study
SSE1-NLuc	*MATa his3Δ1 leu2Δ0 met15Δ0 ura3Δ0 + [pTDH3-SSE1-NLUC-tADH1 URA3]*	This study
SOD1-NLuc	*MATa his3Δ1 leu2Δ0 met15Δ0 ura3Δ0 + [pTDH3-SOD1-NLUC-tADH1 URA3]*	This study
FBA1-NLuc	*MATa his3Δ1 leu2Δ0 met15Δ0 ura3Δ0 + [pTDH3-FBA1-NLUC-tADH1 URA3]*	This study
ADO1-NLuc	*MATa his3Δ1 leu2Δ0 met15Δ0 ura3Δ0 + [pTDH3-ADO1-NLUC-tADH1 URA3]*	This study
SCW10-NLuc	*MATa his3Δ1 leu2Δ0 met15Δ0 ura3Δ0 + [pTDH3-SCW10-NLUC-tADH1 URA3]*	This study
HSP26-NLuc	*MATa his3Δ1 leu2Δ0 met15Δ0 ura3Δ0 + [pTDH3-HSP26-NLUC-tADH1 URA3]*	This study
ALIX-NLuc	*MATa his3Δ1 leu2Δ0 met15Δ0 ura3Δ0 + [pTDH3-ALIX-NLUC-tADH1 URA3]*	This study
TSPAN14-NLuc	*MATa his3Δ1 leu2Δ0 met15Δ0 ura3Δ0 + [pTDH3-TSPAN14-NLUC-tADH1 URA3]*	This study
APOE-NLuc	*MATa his3Δ1 leu2Δ0 met15Δ0 ura3Δ0 + [pTDH3-APOE-NLUC-tADH1 URA3]*	This study
TSPAN2-NLuc	*MATa his3Δ1 leu2Δ0 met15Δ0 ura3Δ0 +*	This study

Strain	Genotype	Source
	[pTDH3-TSPAN2-NLUC-tADH1 URA3]	
TSPAN3-NLuc	*MATa his3Δ1 leu2Δ0 met15Δ0 ura3Δ0 + [pTDH3-TSPAN3-NLUC-tADH1 URA3]*	This study
CD9-NLuc	*MATa his3Δ1 leu2Δ0 met15Δ0 ura3Δ0 + [pTDH3-CD9-NLUC-tADH1 URA3]*	This study
PTGFRN-NLuc	*MATa his3Δ1 leu2Δ0 met15Δ0 ura3Δ0 + [pTDH3-PTGFRN-NLUC-tADH1 URA3]*	This study
MARKCSL1-NLuc	*MATa his3Δ1 leu2Δ0 met15Δ0 ura3Δ0 + [pTDH3-MARKCSL1-NLUC-tADH1 URA3]*	This study
HSPA2-NLuc	*MATa his3Δ1 leu2Δ0 met15Δ0 ura3Δ0 + [pTDH3-HSPA2-NLUC-tADH1 URA3]*	This study
HSP82-NLuc	*MATa his3Δ1 leu2Δ0 met15Δ0 ura3Δ0 + [pTDH3-HSP82-NLUC-tADH1 URA3]*	This study
PGI1-NLuc	*MATa his3Δ1 leu2Δ0 met15Δ0 ura3Δ0 + [pTDH3-PGI1-NLUC-tADH1 URA3]*	This study
PRDX1-NLuc	*MATa his3Δ1 leu2Δ0 met15Δ0 ura3Δ0 + [pTDH3-PRDX1-NLUC-tADH1 URA3]*	This study
HSPA8-NLuc	*MATa his3Δ1 leu2Δ0 met15Δ0 ura3Δ0 + [pTDH3-HSPA8-NLUC-tADH1 URA3]*	This study
CD63-NLuc	*MATa his3Δ1 leu2Δ0 met15Δ0 ura3Δ0 + [pTDH3-CD63-NLUC-tADH1 URA3]*	This study
TAL1-NLuc	*MATa his3Δ1 leu2Δ0 met15Δ0 ura3Δ0 + [pTDH3-TAL1-NLUC-tADH1 URA3]*	This study
TDH1-NLuc	*MATa his3Δ1 leu2Δ0 met15Δ0 ura3Δ0 + [pTDH3-TDH1-NLUC-tADH1 URA3]*	This study
TRX2-NLuc	*MATa his3Δ1 leu2Δ0 met15Δ0 ura3Δ0 + [pTDH3-TRX2-NLUC-tADH1 URA3]*	This study
ADE1-NLuc	*MATa his3Δ1 leu2Δ0 met15Δ0 ura3Δ0 + [pTDH3-ADE1-NLUC-tADH1 URA3]*	This study
ADH1-NLuc	*MATa his3Δ1 leu2Δ0 met15Δ0 ura3Δ0 + [pTDH3-ADH1-NLUC-tADH1 URA3]*	This study
SBA1-NLuc	*MATa his3Δ1 leu2Δ0 met15Δ0 ura3Δ0 + [pTDH3-SBA1-NLUC-tADH1 URA3]*	This study

Strain	Genotype	Source
ENO1-NLuc	*MATa his3Δ1 leu2Δ0 met15Δ0 ura3Δ0 + [pTDH3-ENO1-NLUC-tADH1 URA3]*	This study
EXG1-NLuc	*MATa his3Δ1 leu2Δ0 met15Δ0 ura3Δ0 + [pTDH3-EXG1-NLUC-tADH1 URA3]*	This study
GPP2-NLuc	*MATa his3Δ1 leu2Δ0 met15Δ0 ura3Δ0 + [pTDH3-GPP2-NLUC-tADH1 URA3]*	This study
TIF2-NLuc	*MATa his3Δ1 leu2Δ0 met15Δ0 ura3Δ0 + [pTDH3-TIF2-NLUC-tADH1 URA3]*	This study
TEF1-NLuc	*MATa his3Δ1 leu2Δ0 met15Δ0 ura3Δ0 + [pTDH3-TEF1-NLUC-tADH1 URA3]*	This study
MARCKS-NLuc	*MATa his3Δ1 leu2Δ0 met15Δ0 ura3Δ0 + [pTDH3-MARCKS-NLUC-tADH1 URA3]*	This study
HSC82-NLuc	*MATa his3Δ1 leu2Δ0 met15Δ0 ura3Δ0 + [pTDH3-HSC82-NLUC-tADH1 URA3]*	This study

2.2 Bacterial Strain

Escherichia coli DH5α competent cells (NEB) and *ccd*B Survival 2 T1^{R} *E. coli* (Thermo Fisher Scientific) were used for standard bacterial cloning and plasmid propagation. Selection and growth of *E. coli* were in Lysogeny Broth (LB) medium at 37 °C shaking at 200rpm. The LB medium was supplemented with appropriate antibiotics (carbenicillin, chloramphenicol, or kanamycin). 1.7% bacteriological agar was added when preparing plates.

2.3 Cloning Strategy; Obtaining Scaffold Protein CDS

Human scaffold protein coding sequences (CDS) were taken directly from the Human ORFeome collection v7.1, which has the CDS in a donor vector (pDONR223) (Table 2). The glycerol-stocked bacteria were streaked onto LB, and Spectinomycin (Spec) and colonies from

plates were grown in liquid media with selection for miniprep. Plasmids were isolated using the Qiagen Miniprep Kit. Four human EV scaffold proteins - Alix, HSP90A, HSPA2, PTGFRN, were mutated through a silent mutation to remove internal cut sites to remove or avoid all instances of BsmBI, BsaI, BpiI and NotI recognition sequences for a smooth Golden Gate reaction and synthesized by TWIST Biosciences.

Yeast EV scaffold protein CDSs were amplified from yeast genomic DNA using AccuPrime *Taq* DNA polymerase (Thermo Fisher Scientific) according to the manufacturer's protocol. The primers were designed *in silico* on Geneious Prime (Version 11.0.18+10), each containing the appropriate 5' or 3' attB recombination site and ~20 nucleotides of the CDS (Table 2.2). All primers had a Tm between 53℃ and 57℃. Primers were ordered in 384-well format from Thermo Fisher Scientific and were delivered using an Echo 525 Acoustic Liquid Handler to a destination plate containing PCR mastermix and genomic DNA. Amplification was performed by combining 8.33µl of yeast genome DNA with 8.33µl of AccuPrime *Taq* DNA, and 208 nl of each forward and reverse primer stock at 100µM (dispensed by Echo) and 32.92 µl of water for a 50µl total reaction volume. Five µl of the PCR reaction was run on a 0.8% ethidium bromide gel or 1% agarose gel with SYBR safe to confirm band size, then the remaining PCR reaction was used for PCR cleanup using a 0.7x ratio of magnetic beads to volume of DNA (M1378-00 Mag-Bind® TotalPure NGS, Omega) to yield pure Yeast EV scaffold protein CDSs. DNA purity was measured using the NanoQuant Plate (Tecan).

Table 2. Primers used in this study.

Gene name	Primer direction	Primer sequence (5' to 3')	Position in a 384-well stock plate
SGT2	FWD	GGGGACAAGTTTGTACAAAAAAGCAGGCTTAATGTCAGCATCAAAAGAAGAAATTG	A1
SGT2	RVS	GGGGACCACTTTGTACAAGAAAGCTGGGTTTTGCTTGTTCTCATTGTCTGGT	A3
CYC8	FWD	GGGGACAAGTTTGTACAAAAAAGCAGGCTGTATGAATCCGGGCGGTGA	A5
CYC8	RVS	GGGGACCACTTTGTACAAGAAAGCTGGGTAGTCGTCGTAGTTTTCATCTTC	A7
PIN3	FWD	GGGGACAAGTTTGTACAAAAAAGCAGGCTGGATGTCTGCTTCATTGATTAA	A9
PIN3	RVS	GGGGACCACTTTGTACAAGAAAGCTGGGTGAAAGATATTATTAACAATATCTGA	A11
BMH2	FWD	GGGGACAAGTTTGTACAAAAAAGCAGGCTTTATGTCCCAAACTCGTGAAGA	A13
BMH2	RVS	GGGGACCACTTTGTACAAGAAAGCTGGGTCTTTGGTTGGTTCACCTTGAG	A15
BMH1	FWD	GGGGACAAGTTTGTACAAAAAAGCAGGCTTTATGTCAACCAGTCGTGAAG	A17
BMH1	RVS	GGGGACCACTTTGTACAAGAAAGCTGGGTTCTTTGGTGCTTCACCTTC	A19
YCR051W	FWD	GGGGACAAGTTTGTACAAAAAAGCAGGCTCCATGAACGCTAATATATGGGTG	A21
YCR051W	RVS	GGGGACCACTTTGTACAAGAAAGCTGGGTATTTCTTCTCTTGGAATCTGG	A23
SBA1	FWD	GGGGACAAGTTTGTACAAAAAAGCAGGCTTAATGTCCGATAAAGTTATTAACCC	C1
SBA1	RVS	GGGGACCACTTTGTACAAGAAAGCTGGGTTAGCTTTCACTTCCGGCTC	C3
HSP26	FWD	GGGGACAAGTTTGTACAAAAAAGCAGGCTCCATGTCATTTAACAGTCCATTTTTTG	C5
HSP26	RVS	GGGGACCACTTTGTACAAGAAAGCTGGGTGGTTACCCCACGATTCTTGA	C7
SSA1	FWD	GGGGACAAGTTTGTACAAAAAAGCAGGCTTAATGTCAAAAGCTGTCGGTATT	C9
SSA1	RVS	GGGGACCACTTTGTACAAGAAAGCTGGGTTATCAACTTCTTCAACGGTTG	C11
SSE1	FWD	GGGGACAAGTTTGTACAAAAAAGCAGGCTTAATGAGTACTCCATTTGGTTTAGA	C13
SSE1	RVS	GGGGACCACTTTGTACAAGAAAGCTGGGTTGTCCATGTCAACATCACCTT	C15

HSP104	FWD	GGGGACAAGTTTGTACAAAAAAGCAGGCTTTATGAACGACCAAACGCAATTTA	C17
HSP104	RVS	GGGGACCACTTTGTACAAGAAAGCTGGGTGATCTAGGTCATCATCAATTTCC	C19
SSA2	FWD	GGGGACAAGTTTGTACAAAAAAGCAGGCTCTATGTCTAAAGCTGTCGGTAT	C21
SSA2	RVS	GGGGACCACTTTGTACAAGAAAGCTGGGTTATCAACTTCTTCGACAGTTG	C23
TDH3	FWD	GGGGACAAGTTTGTACAAAAAAGCAGGCTCCATGGTTAGAGTTGCTATTAACGG	E1
TDH3	RVS	GGGGACCACTTTGTACAAGAAAGCTGGGTTAGCCTTGGCAACGTGTTCAA	E3
ENO1	FWD	GGGGACAAGTTTGTACAAAAAAGCAGGCTCGATGGCTGTCTCTAAAGTTTAC	E5
ENO1	RVS	GGGGACCACTTTGTACAAGAAAGCTGGGTCTAATTTGTCACCGTGGTGG	E7
ENO2	FWD	GGGGACAAGTTTGTACAAAAAAGCAGGCTCCATGGCTGTCTCTAAAGTTTACG	E9
ENO2	RVS	GGGGACCACTTTGTACAAGAAAGCTGGGTACAACTTGTCACCGTGGTG	E13
PGK1	FWD	GGGGACAAGTTTGTACAAAAAAGCAGGCTTAATGTCTTTATCTTCAAAGTTGTCTG	E17
PGK1	RVS	GGGGACCACTTTGTACAAGAAAGCTGGGTATTTCTTTTCGGATAAGAAAGCAAC	E19
EXG1	FWD	GGGGACAAGTTTGTACAAAAAAGCAGGCTGGATGCTTTCGCTTAAAACGTTAC	E21
EXG1	RVS	GGGGACCACTTTGTACAAGAAAGCTGGGTCGTTAGAAATTGTGCCACATTG	E23
PDC1	FWD	GGGGACAAGTTTGTACAAAAAAGCAGGCTCGATGTCTGAAATTACTTTGGGTAAA	G1
PDC1	RVS	GGGGACCACTTTGTACAAGAAAGCTGGGTCTTGCTTAGCGTTGGTAGCA	G3
TDH2	FWD	GGGGACAAGTTTGTACAAAAAAGCAGGCTCCATGGTTAGAGTTGCTATTAACGG	G5
TDH2	RVS	GGGGACCACTTTGTACAAGAAAGCTGGGTGAGCCTTGGCAACGTGTTCAA	G7
GPP1	FWD	GGGGACAAGTTTGTACAAAAAAGCAGGCTGGATGCCTTTGACCACAAAACC	G9
GPP1	RVS	GGGGACCACTTTGTACAAGAAAGCTGGGTGCCATTTCAACAAGTCATCCTTA	G11
PDI1	FWD	GGGGACAAGTTTGTACAAAAAAGCAGGCTCCATGAAGTTTTCTGCTGGTGC	G13
PDI1	RVS	GGGGACCACTTTGTACAAGAAAGCTGGGTGCAATTCATCGTGAATGGCATC	G15

ADH1	FWD	GGGGACAAGTTTGTACAAAAAAGCAGGCTTTATG TCTATCCCAGAAACTCAAAA	G17
ADH1	RVS	GGGGACCACTTTGTACAAGAAAGCTGGGTGTTTA GAAGTGTCAACAACGTATC	G19
CDC19	FWD	GGGGACAAGTTTGTACAAAAAAGCAGGCTGGAT GTCTAGATTAGAAAGATTGACC	G21
CDC19	RVS	GGGGACCACTTTGTACAAGAAAGCTGGGTTAAC GGTAGAGACTTGCAAAGT	G23
HSC82	FWD	GGGGACAAGTTTGTACAAAAAAGCAGGCTCCAT GGCTGGTGAAACTTTTGAATT	I1
HSC82	RVS	GGGGACCACTTTGTACAAGAAAGCTGGGTGATC AACTTCTTCCATCTCGG	I3
FBA1	FWD	GGGGACAAGTTTGTACAAAAAAGCAGGCTCCAT GGGTGTTGAACAAATCTTAAA	I5
FBA1	RVS	GGGGACCACTTTGTACAAGAAAGCTGGGTTTAAA GTGTTAGTGGTACGGAA	I7
ADK1	FWD	GGGGACAAGTTTGTACAAAAAAGCAGGCTCGAT GTCTAGCTCAGAATCCATT	I9
ADK1	RVS	GGGGACCACTTTGTACAAGAAAGCTGGGTTTAAA GTGTTAGTGGTACGGAA	I11
SCW4	FWD	GGGGACAAGTTTGTACAAAAAAGCAGGCTGGAT GCGTCTCTCTAACCTAATT	I13
SCW4	RVS	GGGGACCACTTTGTACAAGAAAGCTGGGTGTTC ATTGGATAGAATACCCCA	I15
AHP1	FWD	GGGGACAAGTTTGTACAAAAAAGCAGGCTCCAT GTCTGACTTAGTTAACAAGAA	I17
AHP1	RVS	GGGGACCACTTTGTACAAGAAAGCTGGGTCCAA ATGAGCCAAGACACTTT	I19
PGI1	FWD	GGGGACAAGTTTGTACAAAAAAGCAGGCTGGAT GTCCAATAACTCATTCACTAAC	I21
PGI1	RVS	GGGGACCACTTTGTACAAGAAAGCTGGGTGCATC CATTCCTTGAATTGATTGAT	I23
HSP82	FWD	GGGGACAAGTTTGTACAAAAAAGCAGGCTCCAT GGCTAGTGAAACTTTTGAA	K1
HSP82	RVS	GGGGACCACTTTGTACAAGAAAGCTGGGTGATCT ACCTCTTCCATTTCG	K3
CPR1	FWD	GGGGACAAGTTTGTACAAAAAAGCAGGCTGGAT GTCCCAAGTCTATTTTGATGT	K5
CPR1	RVS	GGGGACCACTTTGTACAAGAAAGCTGGGTGTAAT TCACCGGACTTGGCAA	K7
ADO1	FWD	GGGGACAAGTTTGTACAAAAAAGCAGGCTTCAT GACCGCACCATTGGTA	K9
ADO1	RVS	GGGGACCACTTTGTACAAGAAAGCTGGGTCTTTA GAGTAAGATATTTTTTCGGAA	K11

BGL2	FWD	GGGGACAAGTTTGTACAAAAAAGCAGGCTGGAT GCGTTTCTCTACTACACTC	K13
BGL2	RVS	GGGGACCACTTTGTACAAGAAAGCTGGGTCTGA AAAGTCACAGTCCAAGGA	K15
KAR2	FWD	GGGGACAAGTTTGTACAAAAAAGCAGGCTGGAT GTTTTTCAACAGACTAAGCG	K17
KAR2	RVS	GGGGACCACTTTGTACAAGAAAGCTGGGTCCAAT TCGTCGTGTTCGAAATAA	K19
PHO12	FWD	GGGGACAAGTTTGTACAAAAAAGCAGGCTACAT GTTGAAGTCAGCCGTTTAT	K21
PHO12	RVS	GGGGACCACTTTGTACAAGAAAGCTGGGTACTGT TTTAATAAAGTGTCGTTGTA	K23
THR4	FWD	GGGGACAAGTTTGTACAAAAAAGCAGGCTGGAT GCCTAACGCTTCCCAA	M1
THR4	RVS	GGGGACCACTTTGTACAAGAAAGCTGGGTGTAAT TTCATTTTAGCAAGTTCTTCT	M3
TEF1	FWD	GGGGACAAGTTTGTACAAAAAAGCAGGCTCCAT GGGTAAAGAGAAGTCTCAC	M5
TEF1	RVS	GGGGACCACTTTGTACAAGAAAGCTGGGTCTTTC TTAGCAGCCTTTTGAGC	M7
GPM1	FWD	GGGGACAAGTTTGTACAAAAAAGCAGGCTCCAT GCCAAAGTTAGTTTTAGTTAG	M9
GPM1	RVS	GGGGACCACTTTGTACAAGAAAGCTGGGTGTTTC TTACCTTGGTTGGCAA	M11
GAS3	FWD	GGGGACAAGTTTGTACAAAAAAGCAGGCTCCAT GCAACTATCTAAAAGTATACTAC	M13
GAS3	RVS	GGGGACCACTTTGTACAAGAAAGCTGGGTTGAG TAGAGCAGAAATCAGAC	M15
HXK2	FWD	GGGGACAAGTTTGTACAAAAAAGCAGGCTCCAT GGTTCATTTAGGTCCAAAAAAAC	M17
HXK2	RVS	GGGGACCACTTTGTACAAGAAAGCTGGGTTGAG TAGAGCAGAAATCAGAC	M19
ALD6	FWD	GGGGACAAGTTTGTACAAAAAAGCAGGCTGGAT GACTAAGCTACACTTTGA	M21
ALD6	RVS	GGGGACCACTTTGTACAAGAAAGCTGGGTGCAA CTTAATTCTGACAGCTT	M23
ADE57	FWD	GGGGACAAGTTTGTACAAAAAAGCAGGCTCGAT GCTCAACATTCTCGTTTTAG	O1
ADE57	RVS	GGGGACCACTTTGTACAAGAAAGCTGGGTGGTA AAGCTTAGTTCCGTTTTCA	O3
ASC1	FWD	GGGGACAAGTTTGTACAAAAAAGCAGGCTCCAT GGCATCTAACGAAGTTTTAGT	O5
ASC1	RVS	GGGGACCACTTTGTACAAGAAAGCTGGGTCGTTA GCAGTCATAACTTGCC	O7

SCW10	FWD	GGGGACAAGTTTGTACAAAAAAGCAGGCTACAT GCGTTTTTCAAATTTCCTAAC	O9
SCW10	RVS	GGGGACCACTTTGTACAAGAAAGCTGGGTGATC ACTTGATAGAATACCCC	O11
GUK1	FWD	GGGGACAAGTTTGTACAAAAAAGCAGGCTGGAT GTCCCGTCCTATCGTAA	O13
GUK1	RVS	GGGGACCACTTTGTACAAGAAAGCTGGGTGTTTT TCTGCAAAGATAAAATCCTTC	O15
GPP2	FWD	GGGGACAAGTTTGTACAAAAAAGCAGGCTGCAT GGGATTGACTACTAAACCT	O17
GPP2	RVS	GGGGACCACTTTGTACAAGAAAGCTGGGTGCCAT TTCAACAGATCGTCC	O19
TIF2	FWD	GGGGACAAGTTTGTACAAAAAAGCAGGCTCCAT GTCTGAAGGTATTACTGATA	A2
TIF2	RVS	GGGGACCACTTTGTACAAGAAAGCTGGGTCGTTC AACAAGGTAGCAATGT	A4
ADE1	FWD	GGGGACAAGTTTGTACAAAAAAGCAGGCTCCAT GTCAATTACGAAGACTGAACTG	A6
ADE1	RVS	GGGGACCACTTTGTACAAGAAAGCTGGGTGGTG AGACCATTTAGACCCTGT	A8
TMA19	FWD	GGGGACAAGTTTGTACAAAAAAGCAGGCTCCAT GATTATTTACAAGGATATCTT	A10
TMA19	RVS	GGGGACCACTTTGTACAAGAAAGCTGGGTGGAT CTTTTCTTCCACAATAC	A12
TDH1	FWD	GGGGACAAGTTTGTACAAAAAAGCAGGCTCCAT GATCAGAATTGCTATTAACGGT	A14
TDH1	RVS	GGGGACCACTTTGTACAAGAAAGCTGGGTGAGC CTTGGCAACATATTCGAT	A16
CYC1	FWD	GGGGACAAGTTTGTACAAAAAAGCAGGCTGGAT GACCTACACTACCAGACA	A18
CYC1	RVS	GGGGACCACTTTGTACAAGAAAGCTGGGTGCTC ACAGGCTTTTTTCAAGTAG	A20
YDL124W	FWD	GGGGACAAGTTTGTACAAAAAAGCAGGCTGCAT GTCATTTCACCAACAGTTC	A22
YDL124W	RVS	GGGGACCACTTTGTACAAGAAAGCTGGGTCTACT TTTTGAGCAGCGTAGTT	A24
PHO3	FWD	GGGGACAAGTTTGTACAAAAAAGCAGGCTGCAT GTCATTTCACCAACAGTTC	C2
PHO3	RVS	GGGGACCACTTTGTACAAGAAAGCTGGGTCTACT TTTTGAGCAGCGTAGTT	C4
FPR1	FWD	GGGGACAAGTTTGTACAAAAAAGCAGGCTCCAT GTCTGAAGTAATTGAAGGTA	C6
FPR1	RVS	GGGGACCACTTTGTACAAGAAAGCTGGGTGGTT GACCTTCAACAATTCGA	C8

TRX2	FWD	GGGGACAAGTTTGTACAAAAAAGCAGGCTTGATGGTCACTCAATTAAAATCCGC	C10
TRX2	RVS	GGGGACCACTTTGTACAAGAAAGCTGGGTCTACGTTGGAAGCAATAGCTTG	C12
IPP1	FWD	GGGGACAAGTTTGTACAAAAAAGCAGGCTGGATGACCTACACTACCAGACA	C14
IPP1	RVS	GGGGACCACTTTGTACAAGAAAGCTGGGTTAACAGAACCGGAGATGAAGA	C16
MET6	FWD	GGGGACAAGTTTGTACAAAAAAGCAGGCTTCATGGTTCAATCTGCTGTCTTA	C18
MET6	RVS	GGGGACCACTTTGTACAAGAAAGCTGGGTAATTCTTGTATTGTTCACGGAAG	C20
EGT2	FWD	GGGGACAAGTTTGTACAAAAAAGCAGGCTCCATGAATAAACTATTGTTACATCTAG	C22
EGT2	RVS	GGGGACCACTTTGTACAAGAAAGCTGGGTTCAGCAGAAATGAGATTAACC	C24
SOD1	FWD	GGGGACAAGTTTGTACAAAAAAGCAGGCTCAATGGTTCAAGCAGTCGCAGT	E2
SOD1	RVS	GGGGACCACTTTGTACAAGAAAGCTGGGTGGTTGGTTAGACCAATGACACC	E4
HRI1	FWD	GGGGACAAGTTTGTACAAAAAAGCAGGCTGCATGCCAGCATTATTAAAAAGATT	E6
HRI1	RVS	GGGGACCACTTTGTACAAGAAAGCTGGGTGAGCGTGATATTCAATAACTTC	E8
TAL1	FWD	GGGGACAAGTTTGTACAAAAAAGCAGGCTCTATGTCTGAACCAGCTCAAAAG	E10
TAL1	RVS	GGGGACCACTTTGTACAAGAAAGCTGGGTCAGCGGTAACTTTCTTTTCAATCAA	E12

Table 3. Entry clones used in this study taken from human ORFeome collection v7.1.

Plasmid Name	Gene	Backbone	Plate and Well locations
pDONR223 - APOE	APOE	pDONR223	31044@B03
pDONR223 - ARC	ARC	pDONR223	11030@E08
pDONR223 - ARRDC1	ARRDC1	pDONR223	11062@F04
pDONR223 - CD9	CD9	pDONR223	11004@E11
pDONR223 - CD63	CD63	pDONR223	11030@B12

pDONR223 - CD81	CD81	pDONR223	11020@D05
pDONR223 - FCER1G	FCER1G	pDONR223	31044@H03
pDONR223 - GPI	GPI	pDONR223	11050@H08
pDONR223 - HSPA1A	HSPA1A	pDONR223	11013@G11
pDONR223 - HSPA1A	HSPA1A	pDONR223	11013@G11
pDONR223 - HSPA8	HSPA8	pDONR223	11013@H03
pDONR223 - MARCKS	MARCKS	pDONR223	51004@B12
pDONR223 - MARCKSL1	MARCKSL1	pDONR223	11044@H11
pDONR223 - PRDX1	PRDX1	pDONR223	11003@E03
pDONR223 - TPM3	TPM3	pDONR223	31033@B12
pDONR223 - TSPAN2	TSPAN2	pDONR223	11019@H11
pDONR223 - TSPAN3	TSPAN3	pDONR223	11030@E08
pDONR223 - TSPAN14	TSPAN14	pDONR223	11048@A10

2.4 *In Silico* Design of NLuc Destination Vector and NLuc Expression Clone

Modular cloning (MoClo) is a standardized and hierarchical method that streamlines the construction of plasmids containing one or more transcriptional units through the use of type IIS restriction enzymes. This approach has been widely adopted and further tailored for specific purposes, such as the development of the modular cloning yeast toolkit (MoClo-YTK) for use in *S. cerevisiae* (Lee *et al.*, 2015). In this study, the Nanoluciferase destination vector was made by a Golden Gate reaction of pre-made part plasmids available from MoClo-YTK and newly made part plasmids using the donor plasmid, pYTK001. First, Nanoluciferase CDS (NLuc) was taken from the NanoLuc® Promega pNL1.1 vector and codon optimized for yeast expression using the

IDT codon optimization tool and synthesized by TWIST with BsmBI recognition sites and MoClo-YTK Type 4a overhangs, which are standardized 4-bp sticky ends used to direct part assembly in the modular cloning system. Then, the NLuc fragment was made into a part plasmid by a Golden Gate reaction with pYTK001. The NLuc part plasmid is introduced as a type 4a part and assembled with the other vector components via a Golden Gate reaction using the type IIS restriction enzyme BsmBI. The other parts in the vector include promoter pTDH3, NLuc type 4a part plasmid, and terminator tADH1 into a backbone containing bacterial origin ColE1, and bacterial selection Amp, URA3 *S. cerevisiae* marker, and 2micron yeast origin of replication (Figure 2).

As a control, the NLuc expression clone consisting solely Nanoluc in the transcription unit was made by a Golden Gate reaction using pTDH3, NLuc type 3 part plasmid, and tADH1 into a backbone containing bacterial origin AmpColE1, URA3 *S. cerevisiae* marker, and 2micron yeast origin of replication.

2.5 Assembly of the MoClo NLuc Destination Vector

Golden Gate reactions were prepared as follows:Each 10-µL reaction contained 50 ng plasmid DNA, 1× FastDigest buffer, ATP at 1 mM final, T7 DNA ligase, 3,000 U (NEB, M0318), and BsmBI-v2, 10 U (NEB, R0739); nuclease-free water was added to 10 µL total. Reaction mixtures were then run in a thermocycler using the following programme: 37 °C for 10 mins, 30 cycles of 37 °C for 1 min and 16 °C for 1 min, followed by 37 °C for 15 mins 85 °C for 15 mins. The reaction mixture was then ready for *E. coli* transformation and plated on LB plates with CAM and CARB selection, incubated overnight (O/N) at 37°C. Colonies that appeared were

picked the next day and inoculated O/N for plasmid miniprep, and 10ul of the miniprep sample was sent for sequence validation through Plasmidsaurus.com.

2.6 Synthesis of Entry and Expression Clones

Pure attB-yeast scaffold protein CDS were made into entry clones by combining 20 ng of pDONR221, 20 ng of attB-yeast EV scaffold protein DNA, 0.3 µl of BP Clonase, and 0.3 µl of TE buffer (TTP Labtech). NLuc expression clones were made following the same reaction, but with 60 ng of NLuc destination vector, 20 ng of entry clones, 0.3 µl of LR Clonase, and 0.3 µl of TE buffer for a total reaction volume of 1 µl. The reaction components were dispensed into a 96-well microplate using a Mantis Microfluidic Liquid Handler (Formulatrix). Gateway reactions were incubated at 25°C for 1 hour, then transformed manually by adding 1µl of Gateway reaction mix into 10µl competent *E. coli* DH5α (NEB). The transformed bacteria were manually diluted to 1:10 and 1:100 dilutions and plated using a spot plating protocol on the OT-2 (Opentrons) robot. Isolated colonies were picked using the *E. coli* picking protocol on Qpix Colony Picker, which picked 3 colonies per construct into a manually prepared 96 deep well plate containing 1 mL of LB with kanamycin (KAN) for entry clones or carbenecillin for expression clones and put into a shaking incubator (37°C, 200 rpm) O/N. The next day, 50% glycerol was added to the O/N plate for stocking.

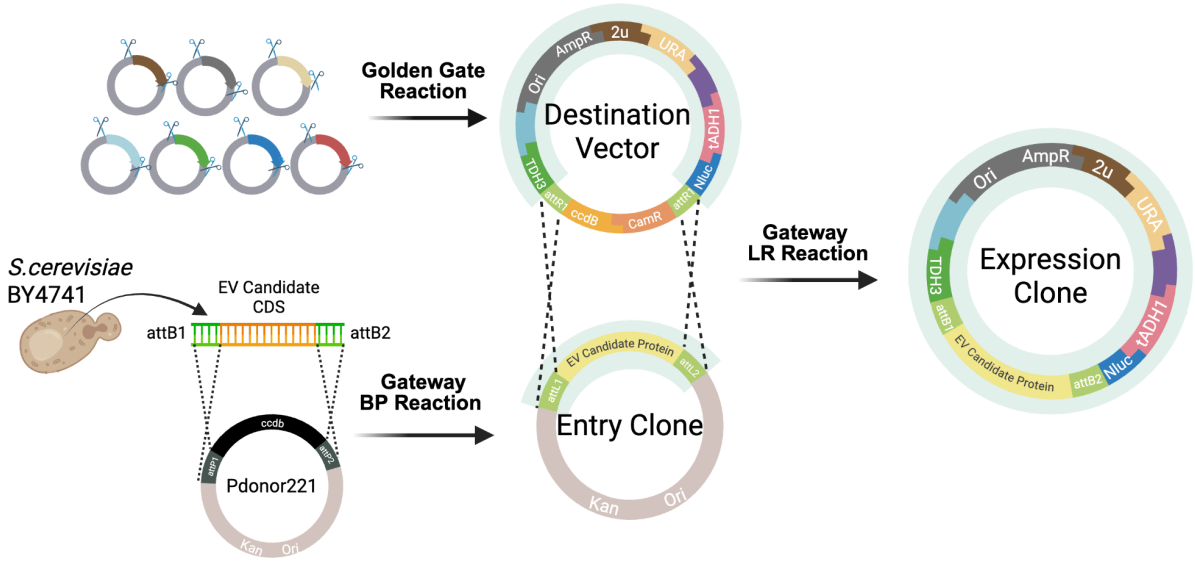
Golden Gate Reaction
Destination Vector
AmpR
2u
URA
tADH1
Nluc
attR
CamR
ccdB
attR
TDH3
Ori
Gateway LR Reaction
Expression Clone
AmpR
2u
URA
tADH1
Nluc
attB2
EV Candidate Protein
attB1
TDH3
Ori
S.cerevisiae
BY4741
EV Candidate CDS
attB1
attB2
Gateway BP Reaction
Entry Clone
EV Candidate Protein
attL1
attL2
Kan
Ori
ccdb
attP1
attP2
Pdonor221
Kan
Ori

Figure 2. Schematic of cloning methodology. Destination vector harbouring NLuc are made using Golden Gate cloning techniques established by the MoClo Yeast Tool Kit (YTK) (Lee et al., 2015). Using LR Gateway cloning, EV candidate scaffold protein parts were transferred into the destination vector as a type 3 position to make the final expression clone containing Candidate proteins N-terminally fused to NLuc.

2.7 Plasmid Minipreps

Colonies grown on either KAN or CARB plates were inoculated into 5 mL of LB medium along with their respective selection and subjected to plasmid extraction using Qiagen's Spin Miniprep Kit (#27104) according to the manufacturer's protocol. DNA concentration was quantified using the Nanodrop Spectrophotometer.

2.8 Plasmid Validation; Pooled PCR

Screening of transformed bacterial colonies was performed by a pooled nanopore sequencing method. Briefly, a single bacterial colony for each construct was included in the pool, each colony inoculated separately in 1 mL in a 96-deep well plate containing LB and antibiotic (KAN or CARB). The plate was put into a shaking incubator (37°C, 200 rpm) O/N. The next day, 30µl of each inoculant was pooled into one 15 mL conical tube containing 5 mL LB broth and grown for 5-6 hours or until ODλ600 ~ 2 (37°C, 200 rpm). The pooled plasmids were then subjected to plasmid extraction as described above, digested using restriction enzymes (SapI for entry clones or NotI for expression clones), which cut once on the plasmid. The linearized plasmids were then purified using the GeneJet PCR cleanup (Thermo Fisher Scientific). The purified and linearized plasmids were sent for sequencing through Plasmidsaurus.com. The raw fragments received by sequencing were then aligned back to the in silico reference plasmid to validate the sequences before transformations.

2.9 Yeast Transformation

Yeast cells were transformed using the lithium acetate protocol. To begin, chemically competent cells were prepared by inoculating a single yeast colony into 5 mL of YPD medium. The culture

was incubated O/N at 30 °C with shaking at 250 rpm until saturated (ODλ600~8-10 or approximately 17–20 hours). The next day, the saturated culture was diluted 1:100 into 5 mL of fresh YPD in a 10 mL test tube and incubated for an additional 4 hours at 30 °C until reaching an ODλ600 of 0.8–1.0, measured with a spectrophotometer.

The cell cultures were then transferred into a 15 mL conical tube and harvested by centrifugation (1000g for 5 mins), washed twice with 5 mL PBS. The cell pellet was resuspended in 500 µL of 0.1 M lithium acetate (LiOAc) and spun at 3000xg for 5 mins. The cells were then resuspended with the transformation mix, which contained salmon sperm DNA (10 mg/mL, Invitrogen), 50% [w/v] polyethylene glycol (PEG), 1M LiOAc and double-distilled water. The cell mix was then aliquoted into Eppendorf tubes containing 2 µL of plasmid DNA. The cell mix was then incubated at 42 °C for 40 mins to facilitate DNA uptake.

After heat shock, cells were pelletted by centrifugation at 3000xg for 5 mins on a tabletop centrifuge, resuspended in 100µL of SD-URA broth and plated onto SD-URA plates. Transformed colonies typically appeared after 3-4 days of incubation at 30 °C.

2.10 Bulk Screening Method to Detect Luminescence in Whole Cell Lysates and Extracellular Media

Nanoluciferase was detected in three sample types: the whole cell lysate, extracellular media post-EV release, and in the isolated EVs. Three colonies of each transformed yeast strain were inoculated into 1 mL of SC-URA in 96 deep well plates, placed into a 30°C shaking incubator overnight or 17-20 hours. The next day, the cells were pelleted by centrifugation at 3750xg on a swinging bucket rotor with plate carriers (Beckman, SX4750) for 5 mins and washed twice with 250 µl PBS (pH 7.4). For WCL NLuc detection, the cells were resuspended in 50ul of DPBS

(Cytiva HyClone™, Fisher Scientific), all of which was then transferred to a 96 white well plate (Falcon®). To detect NLuc activity in WCLs, I used a 1:10 dilution of NanoGlo reagent prepared according to the manufacturer's protocol, diluted with PBS (Cytiva HyClone™, Fisher Scientific) as an initial validation that our strains are expressing NLuc. A 1:1 NanoGlo reagent was used to detect luminescence in the extracellular media.

For extracellular media NLuc detection, the washed cells were resuspended in 200 µl of DBPS (HyClone™, Fisher Scientific) and moved to a 96 flat-bottom plate sealed twice with parafilm and put into a 42 °C water bath for 30 mins following our lab's previous methods to induce EV release. After heat stress, the cells were spun at 3750xg for 15 mins. Then, 100 µl of the supernatant was first transferred into a well of the first 96-well white plate. To ensure homogenization of the extracellular media samples across plates, 50 µl was subsequently transferred from each well of the first plate into the corresponding well of a second 96-well white plate. One plate was treated with NanoGlo's substrate; fluorofurimazine and lysis buffer that contains tritonx100, the other with fluorofurimazine and PBS (Cytiva HyClone™, Fisher Scientific). The luminescence activity was measured on a multimode plate reader (Synergy H1, Biotek) 3 mins after adding the NanoGlo reagent. The reader was set to luminescence mode with an integration time of 1 second per well. Gain was set to 115 but adjusted down to 100 in the case of overluminescence, and the read height was adjusted to 6 mm. Plates were maintained at room temperature during measurements.

2.11 Isolation of EVs by SEC

Yeast strains were initially cultured in 15 mL of yeast peptone dextrose (YPD) medium at 30 °C for 8 hours. Optical density at 600 nm ($OD\lambda_{600}$) was measured after 8 hours and was used to

calculate specific volumes to inoculate into 1L of fresh YPD. The culture was incubated for an additional 17 hours at 30 °C, reaching a final OD_{600} of ~10. Cells were harvested by centrifugation at 3500xg for 10 mins and subjected to mild, sublethal heat stress: incubation at 42 °C for 15 mins, resuspension in 30 mL PBS (Cytiva HyClone™, Fisher Scientific), followed by another 15-minute incubation at 42°C. The suspension was centrifuged at 5,000xg for 15 mins at 4 °C, and the supernatant was collected and further clarified at 15,000x g for 15 mins at 4°C. The resulting supernatant was filtered through a 0.22 µm membrane (Corning Inc.) and ultrafiltered using 10 kDa cut-off spin-filters (Millipore, UFC901024). The retentate from the 10 kDa spin filter was further concentrated by loading 250µl of concentrated supernatant into SEC columns (Izon, SP1) and passing samples through the column by adding 800 µl DPBS. After discarding the void fraction (first 1mL), a total of 2 fractions of the eluate (1 mL per fraction) were collected. The second fraction was labelled as the EV fraction because, based on the manufacturer's size-exclusion chromatography profile, vesicles eluted predominantly in this fraction. The fourth fraction was labelled as the protein fraction as it is enriched in soluble proteins that elute after the vesicles.

2.12 Nanoparticle Tracking Analysis

Nanoparticle tracking analysis was performed to measure the concentration and particle size of EVs isolated from supernatants of heat-shocked cells using the Nanoparticle Tracking Analysis (NTA) ZetaView instrument. EV samples were either undiluted or diluted 1:50 in the same sterile tissue culture grade PBS used to resuspend the initial heat shock pellet. ZetaView instrument settings were as follows: Temperature (25 °C), laser λ (488 nm), Filter λ (scatter) Sens (85), Shutter (100), FR (30), Trace length (15).

2.13 Calculation of RLU in WCL, Secreted and Intravesicular and EVs

All NLuc luminescence data were normalized to the estimated number of cells in the O/N cultures used for the assay. A 1:20 dilution of O/N cultures grown in 96-deep-well plates was prepared in the same medium and transferred to a 96-well flat-bottom plate (FALCON) for OD_{600} measurement using a plate reader. The OD_{600} of the undiluted culture (1:1) was extrapolated, and the measured RLU was then divided by the corresponding cell number, assuming 1 OD_{600} = 1 × 10^7 cells, and the resulting per-cell value was multiplied by 10,000 to yield the RLU per 10,000 cells. The same approach was applied to calculate RLU in extracellular media from 10,000 cells. Intravesicular RLU was determined by subtracting the RLU of samples treated with NanoGlo substrate and PBS from the RLU of samples treated with NanoGlo substrate and NanoGlo buffer containing Triton. Secreted RLU was obtained by subtracting intravesicular RLU from total RLU (measured in the presence of Triton). The percentage of intravesicular RLU was calculated as (intravesicular RLU ÷ total RLU) × 100.

2.14 Data Analysis

Experiments were performed in 2–3 independent replicates, and data are represented as mean ± S.E.M. Statistical analysis was performed by GraphPad Prism (version 10.2.1, GraphPad Software). Comparisons were calculated using a paired t-test. Data generated from ZetaView NTA analysis, shown in Figure 6, were analyzed using ParticleMetrix ZetaView software (version 8.0.5.14 SP7) and Excel. Schematic figures were created with Biorender.com.

Results

3.1 Candidate EV Scaffold Proteins of Interest

To begin, I designed a preliminary workflow to validate the high-throughput cloning pipeline in 96-well plate format and thus required a set of up to 96 candidate genes for proof-of-concept studies. To achieve my second objective, I selected an initial panel of 88 known EV proteins, potential use as scaffold proteins from *S. cerevisiae* (native) and human (ectopic) for expression in yeast (Figure 3), leaving the remaining 8 wells for calibration or control samples. Candidate selection was guided primarily by assessing relative protein abundance, primarily based on published EV proteomics studies, as well as testing existing human scaffolds, EV biomarkers and proteins that confer useful functionalities for potential future applications. As scaffolds have not been identified in yeast, I chose 62 yeast proteins that showed the highest abundance in five independent EV proteomics datasets, most of which have human orthologs also identified in human EV samples, e.g. heat shock protein chaperones (Hsp26, Ssa1 and Sse1), as well as prion-like proteins Cyc8 and Pin3 which may promote clustering of desired cargoes for efficient EV packaging (Kelly et al., 2014, Patel et al., 2009). The 34 human candidates included orthologous heat shock proteins (e.g. HSP90), validated scaffold proteins (CD63, ALIX; studied in human cells), tetraspanin family proteins (CD9, CD81, TSPAN3), common cancer EV biomarkers (TENM2, VDBP, TPM3), proteins implicated in EV biogenesis (ARC, ARRDC1, FLOT1, FCER1G), and proteins found in EV proteomics datasets that had desirable functionalities (PRDX1 for removing reactive oxygen species which helps protect against cellular aging, CLU for tissue regeneration) (Anand et al., 2018; Chen et al., 2025; Luther et al., 2025; Martinez Bravo et al., 2017; Neri et al., 2019; Zhao et al., 2023; Min et al., 2024; He et al.,

2024). Of these candidates, most are soluble proteins for loading attached cargoes into the EV lumen, and others are transmembrane proteins for displaying attached cargoes on the EV surface (Logan et al., 2024). Collectively, this candidate panel captures a diverse set of scaffolds withthe potential to study fundamental EV biology and drive translational applications.

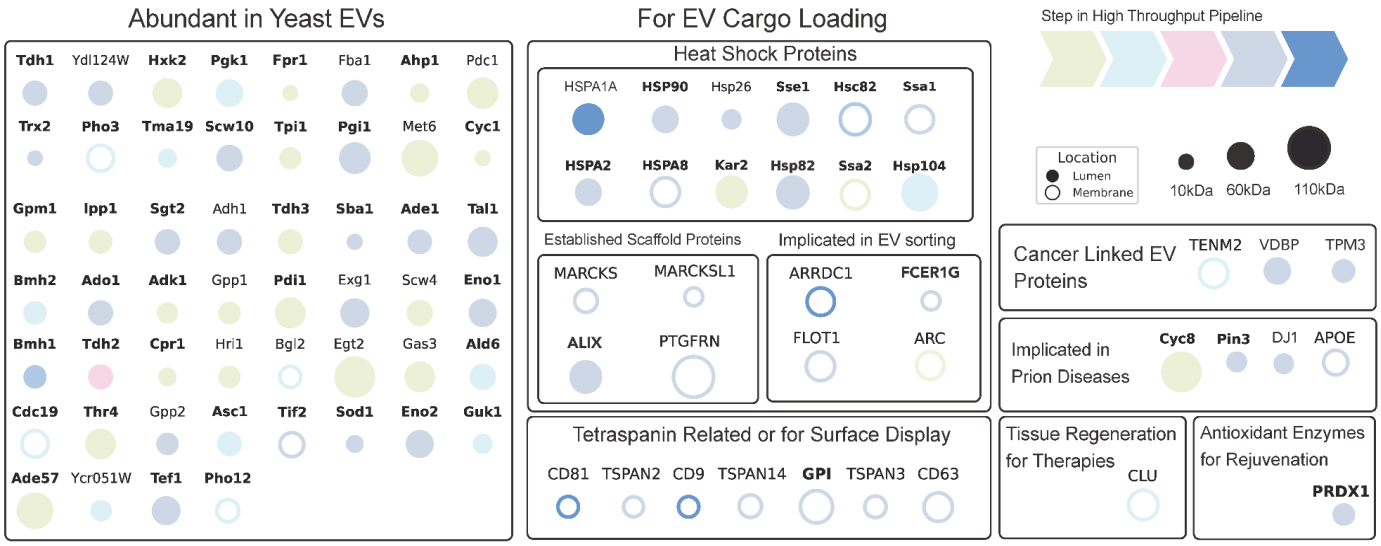
Abundant in Yeast EVs
Tdh1 Ydl124W Hxk2 Pgk1 Fpr1 Fba1 Ahp1 Pdc1
Trx2 Pho3 Tma19 Scw10 Tpi1 Pgi1 Met6 Cyc1
Gpm1 Ipp1 Sgt2 Adh1 Tdh3 Sba1 Ade1 Tal1
Bmh2 Ado1 Adk1 Gpp1 Pdi1 Exg1 Scw4 Eno1
Bmh1 Tdh2 Cpr1 Hri1 Bgl2 Egt2 Gas3 Ald6
Cdc19 Thr4 Gpp2 Asc1 Tif2 Sod1 Eno2 Guk1
Ade57 Ycr051W Tef1 Pho12
For EV Cargo Loading
Heat Shock Proteins
HSPA1A HSP90 Hsp26 Sse1 Hsc82 Ssa1
HSPA2 HSPA8 Kar2 Hsp82 Ssa2 Hsp104
Established Scaffold Proteins
MARCKS MARCKSL1
ALIX PTGFRN
Implicated in EV sorting
ARRDC1 FCER1G
FLOT1 ARC
Tetraspanin Related or for Surface Display
CD81 TSPAN2 CD9 TSPAN14 GPI TSPAN3 CD63
Step in High Throughput Pipeline
Location
Lumen
Membrane
10kDa 60kDa 110kDa
Cancer Linked EV Proteins
TENM2 VDBP TPM3
Implicated in Prion Diseases
Cyc8 Pin3 DJ1 APOE
Tissue Regeneration for Therapies
CLU
Antioxidant Enzymes for Rejuvenation
PRDX1

Figure 3. Overview of the 88 candidate scaffolds used in this proof-of-concept study. Candidate scaffold proteins are categorized by basis on selection. Capitalized protein labels are human proteins, lowercase are *S. cerevisiae*. Proteins that have *S. cerevisiae* and human orthologs in bold type. Circles indicate approximate protein molecular weight (size) and whether the protein is hypothesized to be in the EV membrane (open) or lumen (closed). Colours indicate stage of the high-throughput research pipeline that was achieved in this study: Green, entry clone validated; light Blue, expression clone validated; pink, cell expression validated by NLuc assay; purple, presence in extracellular media validated by NLuc assay; dark blue, presence in EVs validated by NLuc assay (see Figure 4).

3.2 Establishing the Cloning and Phenotyping Pipeline

When designing the cloning protocol, I built upon the existing MoClo Yeast ToolKit (YTK) for a method of plasmid-based strain engineering that allows generation and rearrangement of the transcription unit component using an widely–used open source library of parts (i.e. promotors, terminators, linkers, fluorescent protein tags, selection markers) and incorporated a strategy to easily integrate new EV cargo proteins in place of NLuc fused to validated scaffolds (Lee et al., 2015). This involved placing the NLuc gene at the 3'-end of the candidate scaffold gene in line with previous work that showed a higher probability of bioluminescence detection when NLuc is fused to the C-terminus (Zheng et al., 2023). Placing the NLuc gene in the destination vector allowed me to integrate different scaffold genes upstream using Gateway technology. In the first round of going through the cloning pipeline, starting from step A to F, I was able to make 50 out of 88 individual NLuc strains (Figure 4).

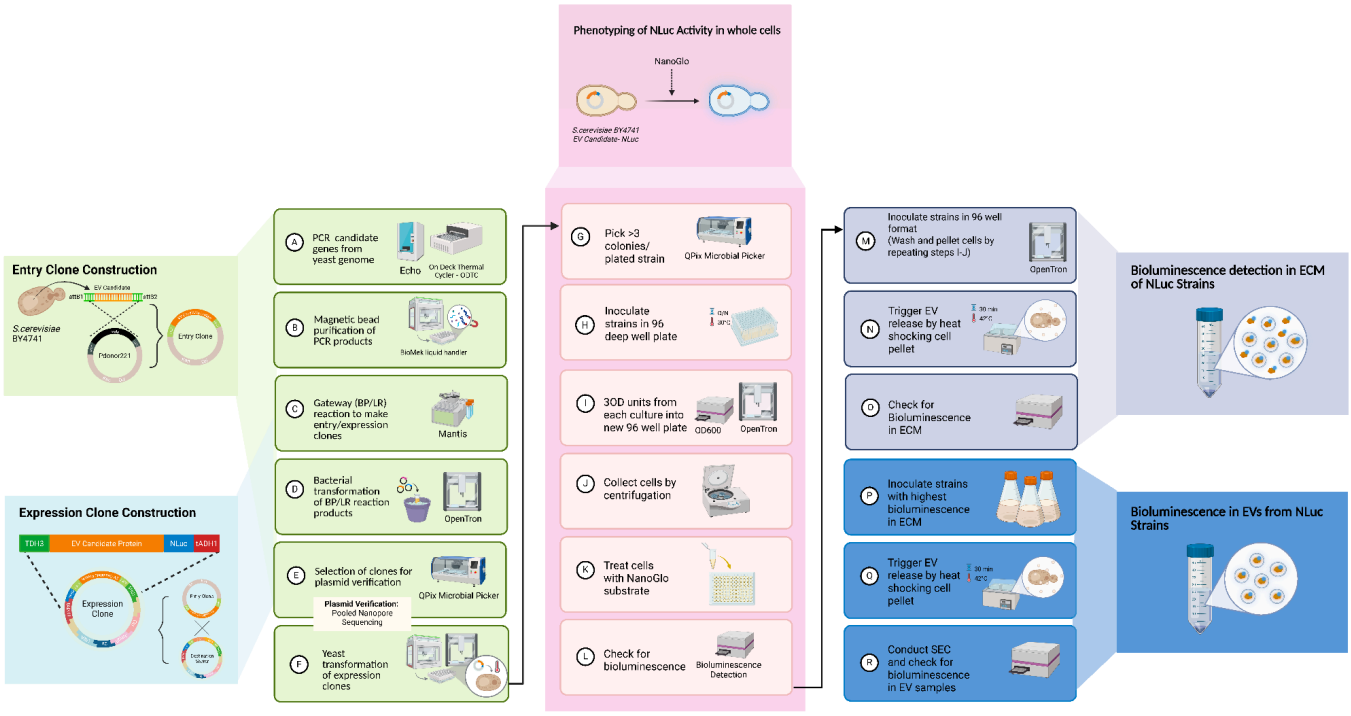
Entry Clone Construction
S.cerevisiae BY4741
Entry Clone
Expression Clone Construction
TDH3
EV Cargoicate Protein
NLuc
tADH1
Expression Clone
A PCR candidate genes from yeast genome
Echo
On Deck Thermal Cycler - ODTC
B Magnetic bead purification of PCR products
BioMek liquid handler
C Gateway (BP/LR) reaction to make entry/expression clones
Mantis
D Bacterial transformation of BP/LR reaction products
OpenTron
E Selection of clones for plasmid verification
QPix Microbial Picker
Plasmid Verification:
Pooled Nanopore Sequencing
F Yeast transformation of expression clones
Phenotyping of NLuc Activity in whole cells
NanoGlo
S.cerevisiae BY4741 EV Candidate- NLuc
G Pick >3 colonies/ plated strain
QPix Microbial Picker
H Inoculate strains in 96 deep well plate
I 30D units from each culture into new 96 well plate
OD600
OpenTron
J Collect cells by centrifugation
K Treat cells with NanoGlo substrate
L Check for bioluminescence
Bioluminescence Detection
M Inoculate strains in 96 well format (Wash and pellet cells by repeating steps I-J)
OpenTron
N Trigger EV release by heat shocking cell pellet
O Check for Bioluminescence in ECM
P Inoculate strains with highest bioluminescence in ECM
Q Trigger EV release by heat shocking cell pellet
R Conduct SEC and check for bioluminescence in EV samples
Bioluminescence detection in ECM of NLuc Strains
Bioluminescence in EVs from NLuc Strains

Figure 4. Optimal workflow for high-throughput yeast genetic engineering and EV phenotyping. Illustration describing the entry vector and expression plasmid construction (left) and procedures and equipment used for semi-automation of *S. cerevisiae* genetic engineering including harvesting, cloning and transforming candidate genes into *S. cerevisiae* (green); transformant screening for whole cell NLuc activity (pink); and candidate scaffold protein NLuc detection in extracellular medium (light blue) and EVs purified by size exclusion chromatography (dark blue) from transformants showing highest NLuc levels. Libraries of entry clone vectors, expression clone plasmids, and yeast strains generated using the robotic equipment shown were cataloged and stored.

3.3 Scaffold Proteins Detected in Yeast Cells and Extracellular Media

To identify scaffold protein-producing yeast transformants, I conducted a phenotyping screen by measuring NLuc activity of whole-cell lysates (WCLs) prepared from 3 clones (colonies) from each of the 50 strains made, selected using Qpix Colony Picker for each candidate. The average NLuc signal for each strain generated (50 total) is shown in Figure 5A. All strains studied had clones with NLuc activity detected over background, i.e. signal from the wild type parent strain BY4741. After confirming scaffold-NLuc protein expression in cells, I collected the extracellular media after heat stress to trigger EV release from these clones and measured luminescence (Figure 5B). Luminescence was detected in extracellular media (treated with detergent) from all strains except CD63, FLOT1, HSPA8, TIF2, TSPAN14, and TSPAN3, which did not exhibit a significant signal over background, suggesting that perhaps the scaffold protein was not released in the ECM through EVs. To determine if the level of cellular expression correlated with the amount of scaffold-NLuc released into the extracellular media, I compared luminescent values from these assays (Figure 5C) and found that at best, some strains released one-tenth of the scaffold-NLuc found in the cell. Among the human EV scaffold candidates, CD81, GPI, HSPA1A, TPM3 and ARRDC1 showed notable EV-mediated release from yeast, suggesting that the machinery that sorts these human scaffolds into EVs may be conserved in yeast. Yeast scaffolds Ado1, Ade1, Hsp82, Hsp26, Hsc82, and Tal1 showed the highest EV-mediated release relative to cellular expression levels. Several candidates – e.g. CD63, FLOT1, TSPAN14, TSPAN3 – exhibited strong expression but limited EV-mediated release, suggesting inefficient EV incorporation. However, based on this screen, most proteins studied are suggested as good candidates as EV scaffolds.

a

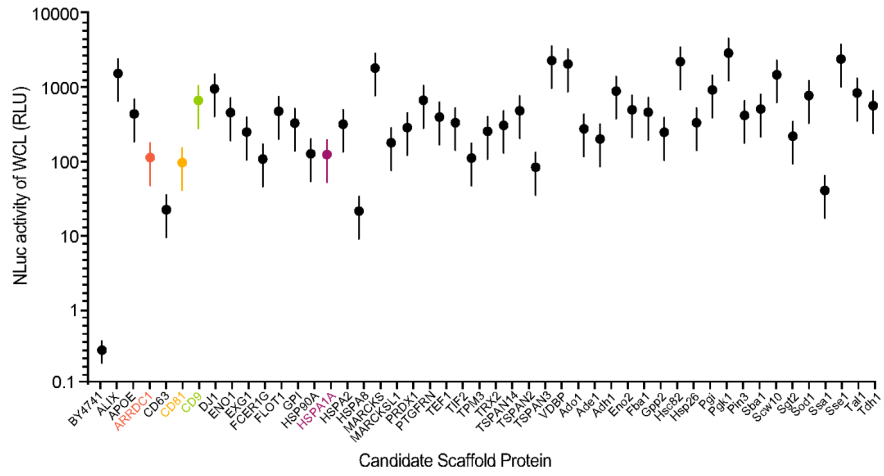
NLuc activity of WCL (RLU)
10000
1000
100
10
1
0.1
BY4741
ALIX
APOE
ARRDC1
CD63
CD81
CD9
DJ1
ENO1
EXG1
FCER1G
FLOT1
GPI
HSP90A
HSPA1A
HSPA2
HSPA8
MARCKS
MARCKSL1
PRDX1
PTGFRN
TEF1
TIF2
TPM3
TRX2
TSPAN14
TSPAN2
TSPAN3
VDBP
Ado1
Ade1
Adh1
Eno2
Fba1
Gpp2
Hsc82
Hsp26
Pgi
Pgk1
Pin3
Sba1
Scw10
Sgt2
Sod1
Ssa1
Sse1
Tal1
Tdh1
Candidate Scaffold Protein

b

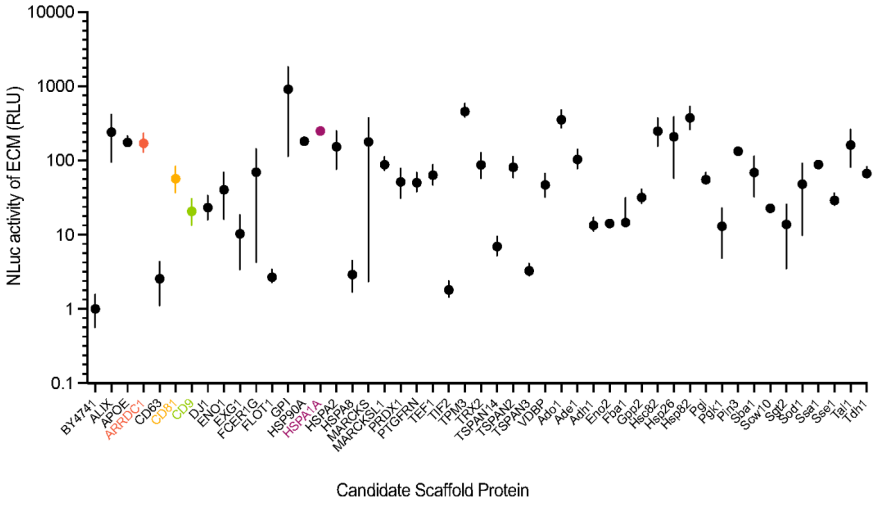
NLuc activity of ECM (RLU)
10000
1000
100
10
1
0.1
BY4741
ALIX
APOE
ARRDC1
CD63
CD81
CD9
DJ1
ENO1
EXG1
FCER1G
FLOT1
GPI
HSP90A
HSPA1A
HSPA2
HSPA8
MARCKS
MARCKSL1
PRDX1
PTGFRN
TEF1
TIF2
TPM3
TRX2
TSPAN14
TSPAN2
TSPAN3
VDBP
Ado1
Ade1
Adh1
Eno2
Fba1
Gpp2
Hsc82
Hsp26
Hsp82
Pgi
Pgk1
Pin3
Sba1
Scw10
Sgt2
Sod1
Ssa1
Sse1
Tal1
Tdh1
Candidate Scaffold Protein

c

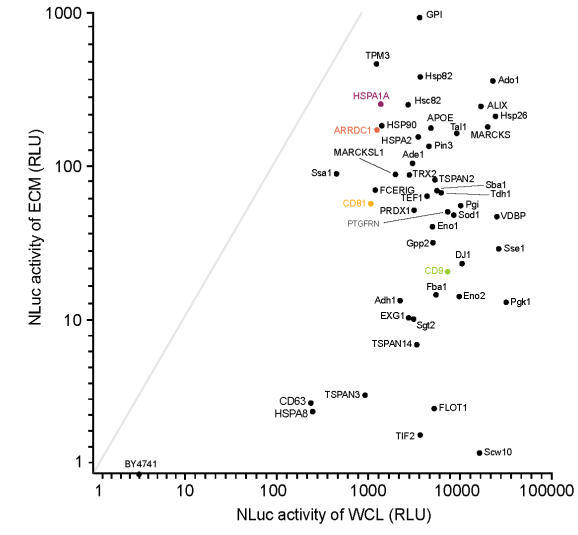
NLuc activity of ECM (RLU)
1000
100
10
1
NLuc activity of WCL (RLU)
1
10
100
1000
10000
100000
GPI
TPM3
Hsp82
Ado1
HSPA1A
Hsc82
ALIX
Hsp26
ARRDC1
HSP90
APOE
Tal1
MARCKS
HSPA2
Pin3
MARCKSL1
Ade1
Ssa1
TRX2
TSPAN2
Sba1
FCER1G
Tdh1
TEF1
CD81
Pgi
PRDX1
Sod1
VDBP
PTGFRN
Eno1
Gpp2
Sse1
DJ1
CD9
Fba1
Adh1
Eno2
Pgk1
EXG1
Sgt2
TSPAN14
CD63
TSPAN3
HSPA8
FLOT1
TIF2
Scw10
BY4741

Figure 5. NLuc activity detected in cell lysates and extracellular media prepared from 50 strains expressing candidate proteins. NLuc activity (normalized in relative luminescence units per 10,000 cells) detected in whole cell lysates (A) or extracellular medium (B) from yeast strains expressing candidate scaffold proteins. (C) Comparison of cell lysate and extracellular media NLuc activity to determine rthe elative amount of candidate proteins secreted. Mean ± S.E.M. shown, $p<0.0001$. The gray line indicates the 1:1 relationship of the RLU between the two variables.

3.4 Some Scaffolds Detected Within Detergent-Soluble Fractions of Extracellular Media Suggesting Presence in EVs

Next, I optimized a phenotyping assay to efficiently screen for potential EV scaffold proteins without having to purify EVs (which requires scaling up culture volumes and using expensive reagents). This involved collecting the extracellular media immediately after driving EV secretion by heat stress (see Logan et al., 2024), splitting the sample into two and treating one with detergent (Triton-X100) to dissolve EV membranes. Luminescence detected in untreated samples represents activity only from soluble secreted scaffold-NLuc (not incorporated into EVs) and scaffolds embedded in EV membranes with NLuc displayed on the exterior EV surface (e.g. Hsp26, FLOT1, Pgk1; Figure 6A). Whereas Triton-X100 treatment will expose protected scaffold-NLuc proteins found in the lumen of EVs to the luciferase substrate, allowing detection of all scaffold proteins in the preparations (Figure 6A).

After conducting measurements, I subtracted luminescence values of Triton-X100-treated samples (total scaffold-NLuc activity) from untreated samples to calculate the proportion of NLuc activity detected with the lumen of EVs (Figure 6B). Consistent with results from experiments conducted without triggered EV release (representing constitutive secretion) shown in Figure 6, I found that most of the top human scaffold candidates (CD9, HSPA2, HSPA1A, MARCKL1, PRDX1, TSPAN2, ARRDC1), except DJ1 and TSPAN3, showed high levels of NLuc activity in intravesicular fractions. Of the top yeast scaffolds, Sod1, Adh1, Ade1, Pin3, Hsc82, YDL14W, and Tal1 showed relatively high intravesicular NLuc activity. Overall, it seemed that the amount of secreted NLuc activity correlated with intravesicular activity,

suggesting that none of the scaffolds studied showed strong enrichment in the EV fractions, but most were detectable.

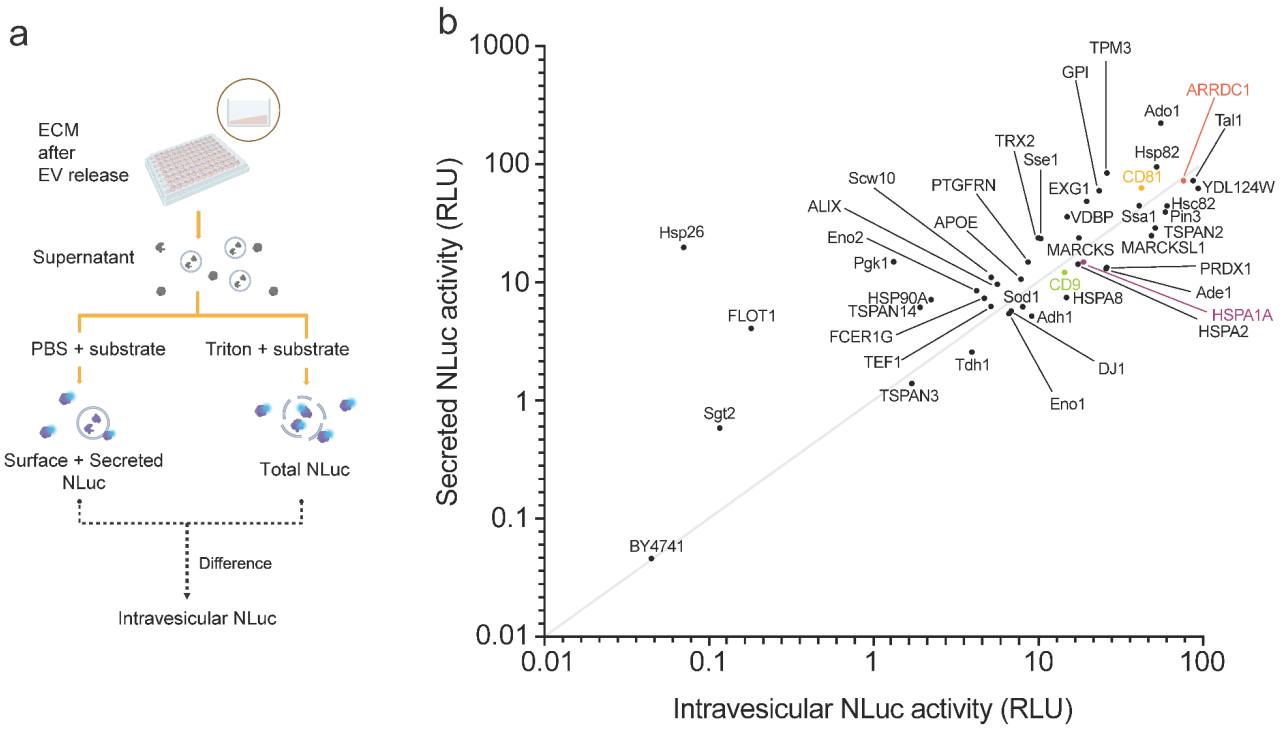
a
ECM
after
EV release
Supernatant
PBS + substrate
Triton + substrate
Surface + Secreted
NLuc
Total NLuc
Difference
Intravesicular NLuc
b
Secreted NLuc activity (RLU)
Intravesicular NLuc activity (RLU)
1000
100
10
1
0.1
0.01
0.01
0.1
1
10
100
TPM3
GPI
ARRDC1
Ado1
Tal1
TRX2
Sse1
Hsp82
CD81
YDL124W
Scw10
PTGFRN
EXG1
Hsc82
ALIX
APOE
VDBP
Ssa1
Pin3
TSPAN2
Hsp26
Eno2
MARCKS
MARCKSL1
Pgk1
PRDX1
CD9
HSP90A
Sod1
HSPA8
Ade1
TSPAN14
Adh1
HSPA1A
FLOT1
FCER1G
HSPA2
TEF1
Tdh1
DJ1
TSPAN3
Eno1
Sgt2
BY4741

Figure 6. Detection of NLuc activity in Detergent-soluble fractions of extracellular media collected from scaffold-expressing strains. (A) Schematic of protocol used to detect total Nluc signal (+ Triton-X100) and soluble secreted and EV surface Nluc signal in extracellular media collected from strains expressing candidate scaffolds. (B) Intravesicular NLuc activity was plotted against secreted NLuc activity (RLU per 10,000 cells). Each dot refers to one strain that expressed a different candidate protein. Colored labels denote strains used for EV isolation experiments (see Figure 7). Mean values are shown (n = 3 biological replicates), p = 0.1356.

3.5 A few Scaffold Proteins Detected in Purified EVs

Results from screening experiments revealed a set of strong scaffold-NLuc candidates that are most likely present at high levels in EVs. I decided to focus on validating the top human scaffold candidates – HSPA1A, ARRDC1, CD9, and CD81 (all with lumenal facing NLuc fusions) – because it would help determine if the EV protein sorting machinery was conserved in yeast, potentially facilitating ectopic expression of other human EV proteins in the future. I isolated EVs from extracellular media collected from these strains after heat stress by ultrafiltration followed by size exclusion chromatography (SEC; Figure 7A). Purified EVs were collected in fraction 2, and I also saved fraction 4, which contains soluble secreted proteins (no EVs), for the detection of NLuc activity.

To assess the size and concentration of EVs in fraction 2, I first conducted nanoparticle tracking analysis (NTA; Figure 7B) and found that expression of the scaffold-NLuc proteins did not affect EV size compared to wild type (~125 nm median diameter; Figure 7C), nor did it affect the number of EVs released (Figure 7D), except for CD81 that showed significantly lower EV release possibly limiting its future use as an EV scaffold protein.

I next measured intralumenal NLuc activity of EV fractions by adding the luminescence substrate with or without Triton-X100 (Figure 7E). I found that EVs isolated from all four strains showed NLuc activity, and the signal was highest for CD9 at ~40% of the total detected (CD9 > HSPA1A > CD81 >> ARRDC1). Finally, I measured total NLuc activity (with detergent) in fraction 2 (EVs) and fraction 4 (soluble proteins) to determine if the candidate scaffold proteins were enriched in EVs (Figure 7F). CD9 was the only candidate that showed significant

enrichment in EVs, whereas CD81 may also be enriched but at low levels, and HSPA1A and ARRDC1 were predominantly found in the soluble protein fraction. Altogether, these results suggest that human CD9 is the best scaffold protein studied, showing high levels of NLuc signal that is enriched in EVs.

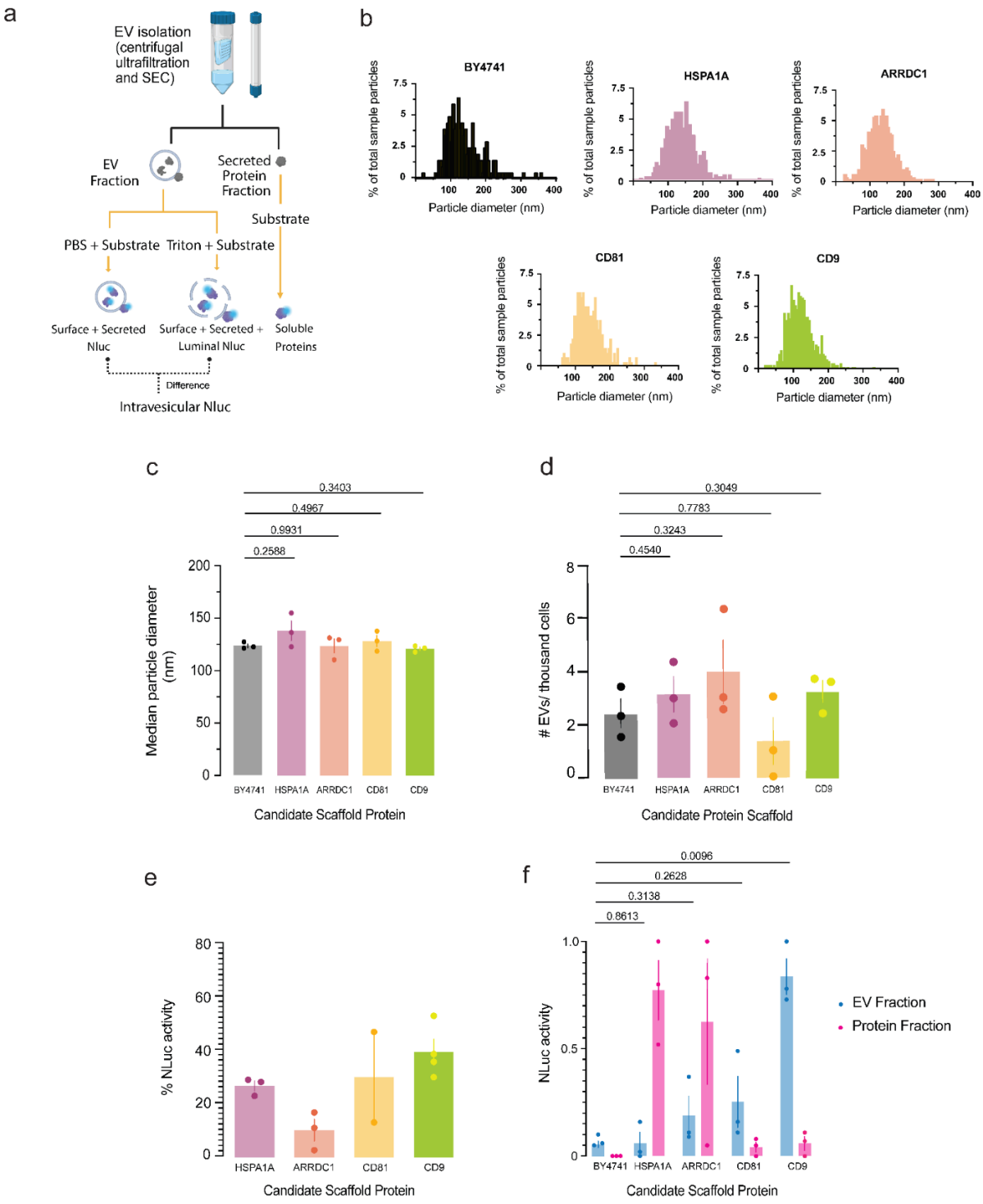
a
EV isolation (centrifugal ultrafiltration and SEC)
EV Fraction
Secreted Protein Fraction
Substrate
PBS + Substrate
Triton + Substrate
Surface + Secreted Nluc
Surface + Secreted + Luminal Nluc
Soluble Proteins
Difference
Intravesicular Nluc
b
BY4741
HSPA1A
ARRDC1
CD81
CD9
% of total sample particles
Particle diameter (nm)
c
Median particle diameter (nm)
0.3403
0.4967
0.9931
0.2588
BY4741
HSPA1A
ARRDC1
CD81
CD9
Candidate Scaffold Protein
d
EVs/ thousand cells
0.3049
0.7783
0.3243
0.4540
Candidate Protein Scaffold
e
% NLuc activity
HSPA1A
ARRDC1
CD81
CD9
Candidate Scaffold Protein
f
NLuc activity
0.0096
0.2628
0.3138
0.8613
EV Fraction
Protein Fraction
Candidate Scaffold Protein

Figure 7. NLuc activity detected in EVs purified from strains expressing four different human scaffold proteins. (A) Schematic of workflow for detecting NLuc activity enriched in EVs purified from extracellular media by ultrafiltration and SEC. (B) Histograms showing the distribution of particle (EV) size across the population of EVs isolated from four strains expressing candidate scaffold proteins and wild type (BY4741), measured using NTA. (C, D) Median particle (EV) diameter (C) and number of EVs released per 1,000 cells (D) for each strain studied, calculated using data obtained by NTA. (E) Intravesicular NLuc activity calculated using 2.5 x 108 EVs from each strain shown. (F) NLuc activity of fraction 2 (EVs) or fraction 4 (soluble secreted) of extracellular media collected from strains shown after SEC. Luminescence values were normalized to the highest signal observed in the sample set (the EV fraction from CD9-NLuc yeast). Mean ± S.E.M. are shown (n = 3 biological replicates). Two-tailed Student's t-tests were used to compare each strain to the wild-type.

Discussion

4.1 Screening for NLuc-tagged EV Scaffolds in *S. cerevisiae*

In summary, I achieved both objectives by successfully implementing a semi-automated, high-throughput workflow to generate a collection of plasmids and genetically modified yeast strains containing candidate EV scaffolds tagged to NLuc and to screen for their presence in cells and detergent-soluble fractions of extracellular media by measuring luminescence. However, because of delays associated with optimizing this challenging workflow, I was unable to phenotype 38 of 88 candidate scaffolds (43%) to keep within the timeframe of my M.Sc. research (< 2 years). Regardless, candidates identified by this proof-of-concept screen were then validated by analyzing purified EVs isolated by SEC, and I found one potentially useful EV scaffold protein, human CD9 (a tetraspanin and human EV biomarker) that exhibited the highest intravesicular signal among all candidates tested.

It is also worth noting that, based on the partial dataset obtained, I observed little to no correlation between cellular and extracellular media NLuc signals for the partial set of candidate fusion proteins studied (see Figure 5C). Nor did I observe a correlation between secreted and intravesicular luminescence signal (Figure 6B). These results are consistent with those reported by Zheng et al., (2023), who also found no correlation between intravesicular luminescence and either cellular or secreted ThermoLuciferase (Tluc) signals when tagged to over 200 different potential human EV scaffolds in HEK293T cells (Zheng et al., 2023). This suggests that not all EV proteins (identified primarily by proteomic analysis of EV samples) will necessarily be efficiently sorted into EVs when overexpressed or when C-terminally fused with a biomarker like luciferase proteins.

Possible explanations for these observations include: (1) NLuc may interfere with the sorting signal of some EV proteins and not others, (2) the machinery responsible for sorting some EV proteins may already be saturated, preventing further loading when these proteins are over-expressed, (3) in the case of some human scaffolds, their sorting signal may not be conserved in yeast, and/or (4) some human scaffolds are observed in EVs only under pathological conditions, which raises the possibility that some scaffolds may require special conditions to be packaged into EVs instead of heat stress, for example, that was employed in this study (see Dixson et al., 2023; Jeon et al., 2025). Furthermore, it was reported that perhaps Tluc enzyme activity or photon lifetime may be diminished in the presence of Triton-X100, which could account for the relatively low intravesicular luminescence signal that was observed (Zheng et al., 2023). In any case, these findings emphasize that EV cargo loading may be context-dependent, and future studies should systematically evaluate how culture conditions, cellular stress, and growth phase may influence the trafficking and secretion of candidate EV scaffold proteins.

4.2 Human CD9 as an EV Scaffold to Efficiently Load Proteins into Yeast EVs

Despite possible limitations mentioned above, this proof-of-concept study identified many potential novel scaffolds that may efficiently drive therapeutic cargo proteins into yeast EVs. These included yeast Sod1, Adh1, Ade1, Pin3, Hsc82, YDL124W, and Tal1 as well as human HSPA2, PRDX1, TSPAN2, MARCKSL1. Notably, human CD9 – a tetraspanin – seems to be highly enriched in yeast EVs and represents the first EV scaffold to be characterized in *S. cerevisiae* that may be used for future engineering experiments.

Moreover, this result suggests that at least some tetraspanin proteins, which are widely studied in mammalian EVs as biomarkers and scaffolds, may be functionally compatible with conserved EV biogenesis machinery within *S. cerevisiae* (Zheng et al., 2023). This result is particularly intriguing because *S. cerevisiae* does not seem to possess any orthologous tetraspanin genes (based on sequence homology). Whereas, human HSPA1A (a heat shock protein 70 kDa member 1A found in EVs released from prostate cancer cells under hypoxic conditions; Diao et al., 2015; Ramteke et al., 2015; Elmallah et al., 2020; Komarova et al., 2021) has a yeast ortholog (Ssa1) but it was not detected within yeast EVs in the study (Figure 7F). Although efficient incorporation of HSPA1A into EVs may require treatment with special conditions (hypoxia), this observation suggests that *S. cerevisiae* may not possess the sorting machinery necessary to package all human scaffolds tested into its EVs. However, all things considered, this work supports the feasibility of leveraging yeast as a heterologous system for screening and engineering EV scaffold proteins.

4.3 Partial Optimization of a Semi-Automated Workflow to Introduce and Phenotype NLuc-tagged EV Scaffolds in Yeast

When developing this semi-automated workflow (see Figure 4), I was unable to construct all entry vectors or expression plasmids with 100% efficiency (i.e. in a single iteration). For example, cloning of most yeast scaffold candidates was stalled at the first step (A, PCR to amply from genomic DNA), preventing their advancement through the cloning pipeline (see Figure 3, candidates shown in green). This is worth noting because even a 99% success rate necessitates additional cloning rounds, increasing both project cost and duration.

Also, traditional clone validation emerged as a major bottleneck, as it was most time-consuming and often unsuccessful during initial test runs. Ultimately, I replaced our original strategy with premium PCR-based sequencing capable of reading linearized DNA fragments. This approach significantly increased throughput by eliminating the need for primer design, manual gel checks, and other conventional benchtop screening steps. However, a recurring challenge was the consistently low DNA yield after digestion and purification. Full insert sequencing of entry vectors remained essential to identify PCR-introduced mutations, and a clear discrepancy threshold was required to ensure consistent acceptance or rejection of clones during validation.

To ensure accuracy and reproducibility at scale, the entire cloning pipeline—from initial PCR to final validation—should be automation-friendly, minimizing human error and enabling precise tracking of plasmid and transformant status and location. After cataloging plasmid and strain generation manually, in the future, I highly recommend informatics support, particularly through a laboratory information management system (LIMS), which will be indispensable for managing future, larger projects and better streamlining data analysis. In addition, I recommend automating routine downstream tasks such as glycerol stocking, restreaking, and inoculation using robotic systems (e.g. Beckman Biomek or Opentron Labworks OT-2) would further improve efficiency and reduce manual labour.

4.4 Additional Future Studies

Throughout this workflow, achieving near 100% efficiency in both entry vector and expression vector construction was critical, as even a 90% success rate could necessitate additional cloning

rounds, increasing both cost and project duration. Clone validation emerged as a major bottleneck, often delaying progression to subsequent stages. Due to these cloning delays, several EV protein constructs were excluded from the current screen. Most yeast EV-tag candidates were stalled during either the amplification step or the entry clone validation step, preventing their advancement through the cloning pipeline.

While the current results support the feasibility of expressing and evaluating human EV proteins in *S. cerevisiae*, further work is needed to determine whether the excluded 38 candidates might outperform the 50 scaffolds tested in this study. Based on their species-specific compatibility, I hypothesize that yeast scafflod candidates will yield higher intravesicular luminescence compared to the human candidates evaluated here. To possibly further improve EV scaffold performance, future experiments should utilize knockout strains lacking the endogenous version of each yeast candidate gene (or the yeast ortholog of the human candidate) encoded in the genome. This approach would prevent competition with native protein, to improve loading into EVs, and clarify the extent to which some scaffold proteins may contribute to yeast EV biogenesis. Future studies should also focus on replacing NLuc tags with proteins of therapeutic value to begin testing potential applications. In addition, the semi-automated high-throughput cloning and phenotyping workflow may be used to generate libraries of hundreds to thousands of yeast strains in support of numerous future studies.

4.5 Conclusion

Beyond identifying at least one new promising EV scaffold protein in *S. cerevisiae,* this study established a versatile platform with broad applications in biotechnology and therapeutic development. By leveraging the exceptional sensitivity of NLuc and its compatibility with high-throughput plate-based assays, the pipeline enables rapid, small-volume phenotyping that can distinguish between whole-cell, extracellular, and EV-localized signals. This is particularly valuable for future engineering of yeast-derived EVs as biological nanocarriers. Reliable yeast-specific EV scaffold proteins could support diverse applications, including targeted protein or RNA delivery, diagnostic platforms where EVs report on intracellular states, and scalable production of therapeutic EVs with reduced batch variability compared to mammalian sources. In future iterations, platform improvements such as multiplexed reporter systems, streamlined separation of free protein versus EV-associated cargo, and fully automated LIMS integration could accelerate EV scaffold discovery. Together, these developments position the established workflow as both a discovery engine for yeast EV biology and a foundation for practical EV-based technologies.

References

Al-Nedawi, K., Meehan, B., Micallef, J., Lhotak, V., May, L., Guha, A., & Rak, J. (2008). Intercellular transfer of the oncogenic receptor EGFRvIII by microvesicles derived from tumour cells. *Nature Cell Biology,* 10(5), 619–624. https://doi.org/10.1038/ncb1725

Alvarez-Erviti, L., Seow, Y., Yin, H., Betts, C., Lakhal, S., & Wood, M. J. A. (2011). Delivery of siRNA to the mouse brain by systemic injection of targeted exosomes. *Nature Biotechnology,* 29(4), 341–345. https://doi.org/10.1038/nbt.1807

Anand, S., Foot, N., Ang, C.-S., Gembus, K. M., Keerthikumar, S., Adda, C. G., Mathivanan, S., & Kumar, S. (2018). Arrestin-Domain Containing Protein 1 (Arrdc1) Regulates the Protein Cargo and Release of Extracellular Vesicles. *PROTEOMICS,* 18(17)*,* 1800266. https://doi.org/10.1002/pmic.201800266

Banks, W. A., Sharma, P., Bullock, K. M., Hansen, K. M., Ludwig, N., & Whiteside, T. L. (2020). Transport of Extracellular Vesicles across the Blood-Brain Barrier: Brain Pharmacokinetics and Effects of Inflammation. *International Journal of Molecular Sciences,* 21(12), Article 12. https://doi.org/10.3390/ijms21124407

Bewicke-Copley, F., Mulcahy, L. A., Jacobs, L. A., Samuel, P., Akbar, N., Pink, R. C., & Carter, D. R. F. (2017). Extracellular vesicles released following heat stress induce bystander effect in unstressed populations. *Journal of extracellular vesicles*, 6(1), 1340746. https://doi.org/10.1080/20013078.2017.1340746

Bobryshev, Y. V., Killingsworth, M. C., & Orekhov, A. N. (2012). Increased Shedding of Microvesicles from Intimal Smooth Muscle Cells in Athero-Prone Areas of the Human Aorta:

Implications for Understanding of the Predisease Stage. *Pathobiology,* 80(1), 24–31. https://doi.org/10.1159/000339430

Chen, J., Lin, J.-J., Wang, W., Huang, H., Pan, Z., Ye, G., Dong, S., Lin, Y., Lin, C., & Huang, Q. (2024). EV-COMM: A database of interspecies and intercellular interactions mediated by extracellular vesicles. *Journal of Extracellular Vesicles,* 13(4)*,* e12442. https://doi.org/10.1002/jev2.12442

Chen, Y., Wang, L., Yu, X., Mao, W., & Wan, Y. (2024). Ultrasonication outperforms electroporation for extracellular vesicle cargo depletion. *Extracellular Vesicle,* 4, *100052.* https://doi.org/10.1016/j.vesic.2024.100052

Chen, Z., Wang, Q., & Lu, Q. (2025). Engineering ARMMs for improved intracellular delivery of CRISPR-Cas9. *Extracellular Vesicle, 5, 100082.* https://doi.org/10.1016/j.vesic.2025.100082

Debbi, L., Guo, S., Safina, D., & Levenberg, S. (2022). Boosting extracellular vesicle secretion Review of Boosting extracellular vesicle secretion. *Biotechnology Advances*, 59, 107983. https://doi.org/10.1016/j.biotechadv.2022.107983

Dixson, A. C., Dawson, T. R., Di Vizio, D., & Weaver, A. M. (2023). Context-specific regulation of extracellular vesicle biogenesis and cargo selection. *Nature Reviews Molecular Cell Biology,* 24(7), 454–476. https://doi.org/10.1038/s41580-023-00576-0

Duport, C., Spagnoli, R., Degryse, E., and Pompon, D. (1998). Self-sufficient biosynthesis of pregnenolone and progesterone in engineered yeast. *Nat. Biotechnol.* 16, 186–189. doi: 10.1038/nbt0298-186

Elashiry, M., Elashiry, M. M., Elsayed, R., Rajendran, M., Auersvald, C., Zeitoun, R., Rashid, M. H., Ara, R., Meghil, M. M., Liu, Y., Arbab, A. S., Arce, R. M., Hamrick, M., Elsalanty, M., Brendan, M., Pacholczyk, R., & Cutler, C. W. (2020). Dendritic cell derived exosomes loaded with immunoregulatory cargo reprogram local immune responses and inhibit degenerative bone disease in vivo. *Journal of Extracellular Vesicles,* 9(1), 1795362. https://doi.org/10.1080/20013078.2020.1795362

Elmallah, M. I. Y., Cordonnier, M., Vautrot, V., Chanteloup, G., Garrido, C., & Gobbo, J. (2020). Membrane-anchored heat-shock protein 70 (Hsp70) in cancer. *Cancer Letters*, 469, 134–141. https://doi.org/10.1016/j.canlet.2019.10.037

Fast, J., Christian, T., Crul, M., Jiskoot, W., Nejadnik, M. R., Medina, A., Radwick, A., Sreedhara, A., & Tole, H. (2024). Use of Closed System Transfer Devices (CSTDs) with Protein-Based Therapeutic Drugs—A Non-Solution for a Non-Problem? *Journal of Pharmaceutical Sciences,* 113(2), 298–305. https://doi.org/10.1016/j.xphs.2023.11.014

Ghodasara, A., Raza, A., Wolfram, J., Salomon, C., & Popat, A. (2023). Clinical Translation of Extracellular Vesicles. *Advanced Healthcare Materials*, 12(28), 2301010. https://doi.org/10.1002/adhm.202301010

Gupta, D., Liang, X., Pavlova, S., Wiklander, O. P. B., Corso, G., Zhao, Y., Saher, O., Bost, J., Zickler, A. M., Piffko, A., Maire, C. L., Ricklefs, F. L., Gustafsson, O., Llorente, V. C., Gustafsson, M. O., Bostancioglu, R. B., Mamand, D. R., Hagey, D. W., Görgens, A., Nordin, J. Z., … El Andaloussi, S. (2020). Quantification of extracellular vesicles in vitro and in vivo using sensitive bioluminescence imaging. Journal of extracellular vesicles, 9(1), 1800222. https://doi.org/10.1080/20013078.2020.1800222

He, J., Ao, C., Li, M., Deng, T., Zheng, S., Zhang, K., Tu, C., Ouyang, Y., Lang, R., Jiang, Y., Yang, Y., Li, C., & Wu, D. (2024). Clusterin-carrying extracellular vesicles derived from human umbilical cord mesenchymal stem cells restore the ovarian function of premature ovarian failure mice through activating the PI3K/AKT pathway. *Stem Cell Research & Therapy,* 15(1), 300. https://doi.org/10.1186/s13287-024-03926-7

Heath, N., Osteikoetxea, X., de Oliveria, T. M., Lázaro-Ibáñez, E., Shatnyeva, O., Schindler, C., Tigue, N., Mayr, L. M., Dekker, N., Overman, R., & Davies, R. (2019). Endosomal Escape Enhancing Compounds Facilitate Functional Delivery of Extracellular Vesicle Cargo. *Nanomedicine,* 14(21), 2799–2814. https://doi.org/10.2217/nnm-2019-0061

Herrmann, I. K., Wood, M. J. A., & Fuhrmann, G. (2021). Extracellular vesicles as a next-generation drug delivery platform. *Nature Nanotechnology*, 16(7), 748–759. https://doi.org/10.1038/s41565-021-00931-2

Hurley, J. H., & Hanson, P. I. (2010). Membrane budding and scission by the ESCRT machinery: It's all in the neck. Nature Reviews. *Molecular Cell Biology,* 11(8), 556–566. https://doi.org/10.1038/nrm2937

Jeon, G., Kim, Y.-H., & Min, J. (2025). Impact of Culture Duration on the Properties and Functionality of Yeast-Derived Extracellular Vesicles. *Biomaterials Research*, 29, 0201. https://doi.org/10.34133/bmr.0201

Johnson, J., Law, S. Q. K., Shojaee, M., Hall, A. S., Bhuiyan, S., Lim, M. B. L., Silva, A., Kong, K. J. W., Schoppet, M., Blyth, C., Ranasinghe, H. N., Sejic, N., Chuei, M. J., Tatford, O. C., Cifuentes-Rius, A., James, P. F., Tester, A., Dixon, I., & Lichtfuss, G. (2023). First-in-human clinical trial of allogeneic, platelet-derived extracellular vesicles as a potential therapeutic for

delayed wound healing. *Journal of Extracellular Vesicles,* 12*,* e12332. https://doi.org/10.1002/jev2.12332

Kang, M., Huang, C.-C., Lu, Y., Shirazi, S., Gajendrareddy, P., Ravindran, S., & Cooper, L. F. (2020). Bone regeneration is mediated by macrophage extracellular vesicles. *Bone,* 141, 115627. https://doi.org/10.1016/j.bone.2020.115627

Kelly, A. C., Busby, B., & Wickner, R. B. (2014). Effect of Domestication on the Spread of the [PIN+] Prion in Saccharomyces cerevisiae. *Genetics*, 197(3), 1007–1024. https://doi.org/10.1534/genetics.114.165670

Lachenal, G., Pernet-Gallay, K., Chivet, M., Hemming, F. J., Belly, A., Bodon, G., Blot, B., Haase, G., Goldberg, Y., & Sadoul, R. (2011). Release of exosomes from differentiated neurons and its regulation by synaptic glutamatergic activity. *Molecular and Cellular Neuroscience,* 46(2), 409–418. https://doi.org/10.1016/j.mcn.2010.11.004

Lässer, C., Eldh, M., & Lötvall, J. (2012). Isolation and characterization of RNA-containing exosomes. *Journal of Visualized Experiments: JoVE, 59,* e3037. https://doi.org/10.3791/3037

LeBleu, V. S., Smaglo, B. G., Mahadevan, K. K., Kirtley, M. L., McAndrews, K. M., Mendt, M., Yang, S., Maldonado, A. S., Sugimoto, H., Salvatierra, M. E., Solis Soto, L. M., Finch, R., Gagea, M., Fluty, A. C., Ludtke, S. J., Lee, J. J., Jain, A. K., Varadhachary, G., Shroff, R. T., … Pant, S. (2025). KRAS G12D -Specific Targeting with Engineered Exosomes Reprograms the Immune Microenvironment to Enable Efficacy of Immune Checkpoint Therapy in PDAC Patients. *medRxiv: The Preprint Server for Health Sciences,* 2025.03.03.25322827. https://doi.org/10.1101/2025.03.03.25322827

Lee, M. E., DeLoache, W. C., Cervantes, B., & Dueber, J. E. (2015). A Highly Characterized Yeast Toolkit for Modular, Multipart Assembly. *ACS Synthetic Biology*, 4(9), 975–986. https://doi.org/10.1021/sb500366v

Lin, Y., Yan, M., Bai, Z., Xie, Y., Ren, L., Wei, J., Zhu, D., Wang, H., Liu, Y., Luo, J., & Li, X. (2022). Huc-MSC-derived exosomes modified with the targeting peptide of aHSCs for liver fibrosis therapy. *Journal of Nanobiotechnology*, 20(1), 432. https://doi.org/10.1186/s12951-022-01636-x

Liu, M., Zhang, Y., He, J., Liu, W., Li, Z., Zhang, Y., Gu, A., Zhao, M., Liu, M., & Liu, X. (2024). Fusion with ARRDC1 or CD63: A Strategy to Enhance p53 Loading into Extracellular Vesicles for Tumor Suppression. *Biomolecules,* 14(5)*,* Article 5. https://doi.org/10.3390/biom14050591

Logan, C. J., Staton, C. C., Oliver, J. T., Bouffard, J., Kazmirchuk, T. D. D., Magi, M., & Brett, C. L. (2024). Thermotolerance in *S. cerevisiae* as a model to study extracellular vesicle biology. *Journal of Extracellular Vesicles*, 13(5), e12431. https://doi.org/10.1002/jev2.12431

Luo, W., Dai, Y., Chen, Z., Yue, X., Andrade-Powell, K. C., & Chang, J. (2020). Spatial and temporal tracking of cardiac exosomes in mouse using a nano-luciferase-CD63 fusion protein. *Communications Biology,* 3(1), 114. https://doi.org/10.1038/s42003-020-0830-7

Luther, K., Navaei, A., Gens, L., Semple, C., Moharil, P., Passalacqua, I., Vyas, K., Wang, Q., Liu, S.-L., Sun, L., Ramaswamy, S., Zocco, D., & Nabhan, J. F. (2025). Scalable production and purification of engineered ARRDC1-mediated microvesicles in a HEK293 suspension cell system. *Scientific Reports,* 15(1), 7299. https://doi.org/10.1038/s41598-025-87674-5

Ma, C.-Y., Zhai, Y., Li, C. T., Liu, J., Xu, X., Chen, H., Tse, H.-F., & Lian, Q. (2024). Translating mesenchymal stem cell and their exosome research into GMP compliant advanced therapy products: Promises, problems and prospects. *Medicinal Research Reviews*, 44(3), 919–938. https://doi.org/10.1002/med.22002

Martínez, J. L., Liu, L., Petranovic, D., & Nielsen, J. (2012). Pharmaceutical protein production by yeast: Towards production of human blood proteins by microbial fermentation. *Current Opinion in Biotechnology,* 23(6), 965–971. https://doi.org/10.1016/j.copbio.2012.03.011

Martinez-Bravo, M.-J., Wahlund, C. J. E., Qazi, K. R., Moulder, R., Lukic, A., Rådmark, O., Lahesmaa, R., Grunewald, J., Eklund, A., & Gabrielsson, S. (2017). Pulmonary sarcoidosis is associated with exosomal vitamin D–binding protein and inflammatory molecules. *Journal of Allergy and Clinical Immunology,* 139(4)*,* 1186–1194. https://doi.org/10.1016/j.jaci.2016.05.051

Mendt, M., Rezvani, K., & Shpall, E. (2019). Mesenchymal stem cell-derived exosomes for clinical use. *Bone Marrow Transplantation*, 54(Suppl 2), 789–792. https://doi.org/10.1038/s41409-019-0616-z

Neri, T., Tavanti, L., De Magistris, S., Lombardi, S., Romei, C., Falaschi, F., Paggiaro, P., & Celi, A. (2019). Endothelial Cell-Derived Extracellular Vesicles as Potential Biomarkers in Chronic Interstitial Lung Diseases. *Annals of Clinical and Laboratory Science,* 49(5)*,* 608–610.

Obuchi, W., Zargani-Piccardi, A., Leandro, K., Rufino-Ramos, D., Di lanni, E., Frederick, D. M., Maalouf, K., Nieland, L., Xiao, T., Repiton, P., Vaine, C. A., Kleinstiver, B. P., Bragg, D. C., Lee, H., Miller, M. A., Breakefield, X. O., & Breyne, K. (2025). Engineering of CD63 Enables Selective Extracellular Vesicle Cargo Loading and Enhanced Payload Delivery. *Journal of Extracellular Vesicles,* 14(6), e70094. https://doi.org/10.1002/jev2.70094

Pacheco-Quinto, J., Clausen, D., Pérez-González, R., Peng, H., Meszaros, A., Eckman, C. B., Levy, E., & Eckman, E. A. (2019). Intracellular metalloprotease activity controls intraneuronal Aβ aggregation and limits secretion of Aβ via exosomes. *The FASEB Journal,* 33(3), 3758–3771. https://doi.org/10.1096/fj.201801319R

Patel, B. K., Gavin-Smyth, J., & Liebman, S. W. (2009). The yeast global transcriptional co-repressor protein Cyc8 can propagate as a prion. *Nature Cell Biology*, 11(3), 344–349. https://doi.org/10.1038/ncb1843

Ramteke, A., Ting, H., Agarwal, C., Mateen, S., Somasagara, R., Hussain, A., Graner, M., Frederick, B., Agarwal, R., & Deep, G. (2015). Exosomes secreted under hypoxia enhance invasiveness and stemness of prostate cancer cells by targeting adherens junction molecules. *Molecular Carcinogenesis,* 54(7), 554–565. https://doi.org/10.1002/mc.22124

Rankin-Turner, S., Vader, P., O'Driscoll, L., Giebel, B., Heaney, L. M., & Davies, O. G. (2021). A call for the standardised reporting of factors affecting the exogenous loading of extracellular vesicles with therapeutic cargos. *Advanced Drug Delivery Reviews,* 173, 479–491. https://doi.org/10.1016/j.addr.2021.04.012

Roohvand, F., Shokri, M., Abdollahpour-Alitappeh, M., & Ehsani, P. (2017). Biomedical applications of yeast- a patent view, part one: Yeasts as workhorses for the production of therapeutics and vaccines. *Expert Opinion on Therapeutic Patents,* 27(8), 929–951. https://doi.org/10.1080/13543776.2017.1339789

Sanghvi, S., Sridharan, D., Evans, P. R., Dougherty, J., Szteyn, K., Gabrilovich, D. I., Dyta, M., Weist, J., Pierre, S. V., Rao, S. G., Halm, D. R., Chen, T., Athanasopoulos, P. S., Dolga, A. M., Yu, L., Khan, M., & Singh, H. (2025). Functional large-conductance calcium and voltage-gated

potassium channels in extracellular vesicles act as gatekeepers of structural and functional integrity. *Nature Communications*, *16*(1). https://doi.org/10.1038/s41467-024-55379-4

Shi, F., Shi, H., Phillips, S., Zhang, B., Ayyaswamy, S., Bryan, R., & Durgan, D. (2021). Examining the role of extacellular vesicles in blood pressure regulation. *The FASEB Journal,* 35(S1). https://doi.org/10.1096/fasebj.2021.35.S1.03850

Smyth, T., Kullberg, M., Malik, N., Smith-Jones, P., Graner, M. W., & Anchordoquy, T. J. (2015). Biodistribution and Delivery Efficiency of Unmodified Tumor-Derived Exosomes. *Journal of Controlled Release : Official Journal of the Controlled Release Society,* 199, 145–155. https://doi.org/10.1016/j.jconrel.2014.12.013

Song, L. L., Tang, Y. P., Qu, Y. Q., Yun, Y. X., Zhang, R. L., Wang, C. R., Wong, V. K. W., Wang, H. M., Liu, M. H., Qu, L. Q., Wu, J. H., Lo, H. H., & Law, B. Y. K. (2025). Exosomal delivery of rapamycin modulates blood-brain barrier penetration and VEGF axis in glioblastoma. *Journal of Controlled Release*, 381, 113605. https://doi.org/10.1016/j.jconrel.2025.113605

Tang, B., Zeng, W., Song, L. L., Wang, H. M., Qu, L. Q., Lo, H. H., Yu, L., Wu, A. G., Wong, V. K. W., & Law, B. Y. K. (2022). Extracellular Vesicle Delivery of Neferine for the Attenuation of Neurodegenerative Disease Proteins and Motor Deficit in an Alzheimer's Disease Mouse Model. *Pharmaceuticals (Basel, Switzerland)*, 15(1), 83. https://doi.org/10.3390/ph15010083

Théry, C., Regnault, A., Garin, J., Wolfers, J., Zitvogel, L., Ricciardi-Castagnoli, P., Raposo, G., & Amigorena, S. (1999). Molecular characterization of dendritic cell-derived exosomes. Selective accumulation of the heat shock protein hsc73. *The Journal of Cell Biology,* 147(3), 599–610. https://doi.org/10.1083/jcb.147.3.599

Trantas, E., Panopoulos, N., & Ververidis, F. (2009). Metabolic engineering of the complete pathway leading to heterologous biosynthesis of various flavonoids and stilbenoids in Saccharomyces cerevisiae. *Metabolic Engineering,* 11(6), 355–366. https://doi.org/10.1016/j.ymben.2009.07.004

Wu, H., Fan, H., Shou, Z., Xu, M., Chen, Q., Ai, C., Dong, Y., Liu, Y., Nan, Z., Wang, Y., Yu, T., & Liu, X. (2019). Extracellular vesicles containing miR-146a attenuate experimental colitis by targeting TRAF6 and IRAK1. *International Immunopharmacology,* 68*,* 204–212. https://doi.org/10.1016/j.intimp.2018.12.043

Yang, J., Liu, X.-X., Fan, H., Tang, Q., Shou, Z.-X., Zuo, D.-M., Zou, Z., Xu, M., Chen, Q.-Y., Peng, Y., Deng, S.-J., & Liu, Y.-J. (2015). Extracellular Vesicles Derived from Bone Marrow Mesenchymal Stem Cells Protect against Experimental Colitis via Attenuating Colon Inflammation, Oxidative Stress and Apoptosis. *PLOS ONE,* 10(10), e0140551. https://doi.org/10.1371/journal.pone.0140551

Zhao, Y.-C., Wang, T.-J., Qu, G.-H., She, L.-Z., Cui, J., Zhang, R.-F., & Qu, H.-D. (2023). TPM3: A novel prognostic biomarker of cervical cancer that correlates with immune infiltration and promotes malignant behavior in vivo and in vitro. *American Journal of Cancer Research,* 13(7), 3123–3139.

Zheng, W., Rädler, J., Sork, H., Niu, Z., Roudi, S., Bost, J. P., Görgens, A., Zhao, Y., Mamand, D. R., Liang, X., Wiklander, O. P. B., Lehto, T., Gupta, D., Nordin, J. Z., & El Andaloussi, S. (2023). Identification of scaffold proteins for improved endogenous engineering of extracellular vesicles. *Nature Communications*, 14(1), 4734. https://doi.org/10.1038/s41467-023-40453-0